An experimental and theoretical determination of oxygen isotope fractionation in the system magnetite-H₂O from 300 to 800°C

DAVID R. COLE,[1,]* JUSKE HORITA,[1] VENIAMIN B. POLYAKOV,[2] JOHN W. VALLEY,[3] MICHAEL J. SPICUZZA,[3] and DOROTHY W. COFFEY[4]

[1]Chemical Sciences Division, Oak Ridge National Laboratory, Oak Ridge, Tennessee 37831, USA
[2]Vernadsky Institute of Geochemistry and Analytical Chemistry, Moscow B-334 Russia
[3]Department of Geology and Geophysics, University of Wisconsin, Madison, Wisconsin 53706, USA
[4]Metals and Ceramics Division, Oak Ridge National Laboratory, Oak Ridge, TN 37831, USA

Abstract—Oxygen isotope fractionations have been determined between magnetite and water from 300 to 800°C and pressures between 10 and 215MPa. We selected three reaction pathways to investigate fractionation: (a) reaction of fine-grained magnetite with dilute aqueous NaCl solutions; (b) reduction of fine-grained hematite through reaction with dilute acetic acid; and (c) oxidation of fine iron power in either pure water or dilute NaCl solutions. Effective use of acetic acid was limited to temperatures up to about 400°C, whereas oxide-solution isotope exchange experiments were conducted at all temperatures. Equilibrium $^{18}O/^{16}O$ fractionation factors were calculated from the oxide-water experiments by means of the partial isotope exchange method, where generally four isotopically different waters were used at any given temperature. Each run product was characterized by X-ray diffraction (XRD), scanning electron microscopy (SEM), and on a limited basis, high-resolution transmission electron microscopy (HRTEM) and Mössbauer spectroscopy. Results from the microscopic examinations indicate the formation of well-crystallized octahedra and dodecahedra of magnetite where the extent of crystallization, grain size, and grain habit depend on the initial starting material, P, T, solution composition, and duration of the run.

The greatest amount of oxygen isotope exchange (~90% or greater) was observed in experiments where magnetite either recrystallized in the presence of 0.5 m NaCl from 500 to 800°C or formed from hematite reacted with 0.5 m acetic acid at 300, 350 and 400°C. Fractionation factors ($10^3 \ln \alpha_{mt-H_2O}$) determined from these partial exchange experiments exhibit a steep decrease (to more negative values) with decreasing temperature down to about 500°C, followed by shallower slope. A least-squares regression model of these partial exchange data, which accounts for analytical errors and errors generated by mass balance calculations, gives the following expression for fractionation that exhibits no minimum: $1000 \ln \alpha_{mt-w} = -8.984(\pm0.3803)x + 3.302(\pm0.377)x^2 - 0.426(\pm0.092)x^3$ with an $R^2 = 0.99$ for $300 \le T \le 800°C$ ($x = 10^6/T^2$). The Fe oxidation results also exhibit this type of temperature dependence but shifted to slightly more negative $10^3 \ln \alpha$ values; there is the suggestion that a kinetic isotope effect may contribute to these fractionations. A theoretical assessment of oxygen isotope fractionation using β-factors derived from heat capacity and Mössbauer temperature (second-order Doppler) shift measurements combined with known β-factors for pure water yield fractionations that are somewhat more negative compared to those determined experimentally. This deviation may be due to the combined solute effects of dissolved magnetite plus NaCl (aq), as well as an underestimation of β_{mt} at low temperatures. The new magnetite-water experimental fractionations agree reasonably well with results reported from other experimental studies for temperatures $\ge 500°C$, but differ significantly with estimates based on quasi-theoretical and empirical approaches. Calcite-magnetite and quartz-magnetite fractionation factors estimated from the combination of magnetite β's calculated in this study with those for calcite and quartz reported by Clayton and Kieffer (1991) agree very closely with experimentally determined mineral-pair fractionations. *Copyright © 2004 Elsevier Ltd*

1. INTRODUCTION

Determination of the distribution of the stable isotopes of O-H-C-S in fluids and minerals has become a standard and extremely powerful approach in elucidating the temperatures, material fluxes, rock and fluid origins, and time scales associated with ancient and active fluid-rock interaction processes in the Earth's crust (see for example, Taylor, 1997; Valley and Cole, 2001). Equilibrium isotope fractionation factors and rates of isotopic exchange form the cornerstones for interpretation of stable isotope data from natural systems. Because of recent

advances in analytical techniques (e.g., high-precision on small sample sizes or *in situ* spots; e.g., Valley et al., 1998), the need for accurate, reliable fractionation factors and rate constants has never been greater. A great deal of progress has been made in determining the equilibrium fractionations of $^{18}O/^{16}O$, D/H, $^{13}C/^{12}C$, and $^{34}S/^{32}S$ among fluid and mineral components at elevated temperatures and pressures from experimental exchange studies, theoretical calculations, and semiempirical estimation methods (e.g., Chacko, 1993; Criss, 1999; Chacko et al., 2001).

Despite the improvements in analytical, experimental, and computational methods, there are still a significant number of rock-forming phases for which fractionation data are limited or

---

* Author to whom correspondence should be addressed (coledr@ornl.gov).

in disagreement. This is particularly true for magnetite, an important accessory mineral occurring in a wide variety of geological and industrial environments. In principle, the oxygen isotope compositions of coexisting mineral pairs, including magnetite and either silicates or carbonates, constitute extremely sensitive isotope geothermometers, particularly in the temperature range relevant to fluid-rock interaction in deep sedimentary basins, geothermal reservoirs, and magma-hydrothermal systems (~100–700°C). Magnetite-water isotope fractionations can also be used to determine fluid sources and origins of secondary magnetite in natural and industrial settings. As will be detailed below, the oxygen isotope fractionation curves for magnetite-water illustrate very clearly the significant discrepancies that occur in the literature between the various empirical, experimental, and quasi-theoretical estimates of the value of fractionation factors, particularly at lower temperatures.

Our objectives in this paper are threefold. First, we present new experimental oxygen isotope fractionation data for magnetite-water over the temperature range of 300 to 800°C. Second, we present new theoretical fractionation factors based on consideration of the thermodynamic properties of magnetite and water. Third, we compare the fractionations obtained in this study to previously reported theoretical, experimental, and empirical calibrations for magnetite-water and mineral-magnetite.

2. PREVIOUS WORK

The oxygen isotope fractionation factors currently available in the literature for magnetite-water or magnetite-mineral pairs fall into four broad categories: (1) empirical, (2) semiempirical, (3) theoretical, and (4) experimental. In some cases, results from two or more of these methods have been combined to formulate a relationship between isotopic fractionation and temperature.

Empirically derived fractionations based on the isotopic compositions of minerals in natural samples and independent estimates of temperature for these samples have been described by Bottinga and Javoy (1975) and Blattner et al. (1983). Bottinga and Javoy (1975) used data from both igneous and metamorphic systems to derive the temperature dependence of oxygen isotope fractionation between magnetite and feldspar (An$_{60}$). Blattner et al. (1983) combined the oxygen isotope compositions of millimeter thick surface layers of magnetite formed in steam pipelines at the Wairakei geothermal power station with isotopic values for the water to calibrate the magnetite-waters fractionations at two temperatures, 112 and 175°C.

Richter and Hoernes (1988), Zheng (1991, 1995), and Hoffbauer et al. (1994) used modifications of the increment method developed by Schütze (1980) to determine fractionation factors for magnetite-water. These semiempirical calibrations are based on the premise that fractionation behavior can be predicted quantitatively from the number of different bond types in the mineral structure (e.g., Fe^{2+}-O; Fe^{3+}-O). The method assigns ^{18}O increments to each type of cation-oxygen bond in the mineral structure and then calculates a weighted average for the mineral as a whole. This relative ^{18}O/^{16}O scale can be linked to an absolute scale using some independently determined fractionation factors. Zheng (1991, 1995) used reduced

partition function ratios of quartz (Si-O) from Kieffer (1982), modified by Clayton et al. (1989), as the reference in calculating the ^{18}O indices of the metal oxides.

Calculations involving the vibrational spectra of minerals and the methods of statistical mechanics have proved successful in producing estimated fractionations for a number of important minerals (e.g., Kieffer, 1982). Magnetite was not included in the calculations of Kieffer (1982) because its opacity prevents adequate spectroscopic determination of its vibrational spectrum (Clayton and Kieffer, 1991). Upper and lower limits to the isotopic partition function ratios were calculated for magnetite by Becker (1971) using constraints set by a combination of low-temperature heat capacity data for the acoustic modes and a single Einstein frequency to represent the unknown vibrational frequencies. The values for the frequencies were chosen to fit experimental magnetite-water fractionations of O'Neil and Clayton (1964) at 700 and 800°C. A similar approach was adopted by Clayton and Kieffer (1991), who reported new estimates for the magnetite partition function ratios. More recently, Polyakov and coworkers (e.g., Polyakov, 1997; Polyakov, 1998; Polyakov and Mineev, 2000; Polyakov et al., 2001) have described a method that combines heat capacity and Mössbauer temperature-shift measurements to calculate reduced partition functions for light elements such as S and O.

Experimentally based calibrations for magnetite-water or magnetite-calcite fractionation are restricted to temperatures of 300°C and above. O'Neil (1963) investigated the fractionations between magnetite and water at 500°C, 700°C, and 800°C using two isotopically different waters. He also measured isotopic fractionations between magnetite and water for systems where magnetite formed from a chemical reaction between siderite and H$_2$O. These results are also given in graphical form in O'Neil and Clayton (1964). Bertenrath et al. (1973) used a similar approach, except they examined magnetite formed from the reduction of hematite with water under controlled oxidation state conditions (Ni-NiO) at temperatures between 300 and 960°C. The details of these experiments are not known because their results are published in abstract form only. Matthews (1976) measured magnetite-water fractionations at 560°C for two different reaction pathways: reduction of hematite with iron, and oxidation of iron. Downs et al. (1981) measured the partitioning of oxygen isotopes between quartz and magnetite at 600 and 800°C and 500 MPa, using an internally heated pressure vessel with a Shaw-membrane. Through adjustment of the hydrogen fugacity, the starting material, fayalite, was decomposed to form quartz and magnetite. The isotopic composition difference between separated quartz and magnetite was measured directly. Chiba et al. (1989) measured the oxygen isotope fractionations involving magnetite and calcite at high pressures (1500 MPa) and temperatures (800°C, 1000°C, 1200°C) using the carbonate-exchange technique of Clayton et al. (1989). More recently, Fortier et al. (1995) used the partial exchange method of Northrop and Clayton (1966) to investigate the fractionation between magnetite and water at 350°C. In this study, hematite was converted to magnetite through reaction with dilute acetic acid solutions (HAc).

A number of studies combined two or more approaches to estimate magnetite-water and magnetite-mineral fractionations. Bottinga and Javoy (1973) and Javoy (1977) combined theo-

Table 1. Oxygen isotope ratios ($\delta^{18}O_{VSMOW}$ in ‰) of starting materials.

Starting Hematite (H)		9.75	($\pm$0.08)	($n = 6$)
Starting Magnetite (M)		8.85	($\pm$0.08)	($n = 5$)
Starting Magnetite (m)		5.04	($\pm$0.09)	($n = 3$)
Waters	W-1-0.1; W-1-0.5; W-1a	−7.52	($\pm$0.00)	($n = 2$)
	W-2-0.1; W-2a	48.27	($\pm$0.04)	($n = 2$)
	W-3-0.5; W-3a	23.52	($\pm$0.05)	($n = 2$)
	W-4-0.1; W-4a	−36.97	($\pm$0.07)	($n = 4$)
	W-6-0.1	12.87	($\pm$0.08)	($n = 2$)
	W-7-0.1; W-7-0.5	2.07	($\pm$0.02)	($n = 3$)
	W-8-0.5	−14.53	($\pm$0.01)	($n = 3$)
	VSMOW	0.00 (NIST standard)		

M = Johnson Matthey Fe$_3$O$_4$, Lot # 21173; m = Johnson Matthey Fe$_3$O$_4$, Lot #S.92743A; n = number of analyses; errors are in 1σ; 0.1 and 0.5 refers to waters with 0.1 and 0.5 molal NaCl, respectively; a = refers to waters with 0.5 molal acetic acid (HAc).

retical and empirical methods to estimate magnetite-water fractionation. O'Neil and Clayton (1964) extrapolated their high-temperature experimental data to low-temperature using an empirical value based on the isotopic compositions of magnetite "teeth" (*Cryptochiton stelleri*) and its coexisting water. Rowe et al. (1994) combined theoretical, experimental, and empirical estimates to construct a magnetite-water curve from 0 to 300°C.

3. MATERIAL AND METHODS

3.1. Reaction Pathways

The ideal isotope exchange experiment is one in which recrystallization is avoided and all isotopic exchange occurs by diffusion (Chacko et al., 1999). Experimentally, this is difficult to accomplish with refractory phases such as magnetite, where diffusion coefficients are low and chemically controlled reaction rates are also very sluggish. The novel carbonate-exchange method developed by Clayton et al. (1989) takes advantage of high temperatures (>800°C) and pressures (1500 MPa) where diffusion rates are fast enough to facilitate exchange. However, for most phases including magnetite, this approach has a rather high temperature cut-off (~600°C). Historically, a variety of reaction pathways have been used to enhance isotopic exchange between magnetite and water. All of these involved some kind of synthesis or recrystallization process; great caution must be used in interpreting the experimental results because the isotopic distribution may be determined by kinetic (i.e., nonequilibrium) isotope effects associated with formation of a new phase. The pathways of choice that involved manipulation of the redox conditions include: (1) oxidation of iron (Matthews, 1976), (2) reduction of hematite (Bertenrath et al., 1973; Matthews, 1976), (3) fayalite breakdown to magnetite and quartz under controlled oxidation conditions (Downs et al., 1981), (4) partial oxidation of iron carbonate with water (O'Neil, 1963), and (5) magnetite recrystallization (O'Neil, 1963). At 350°C, Fortier et al. (1995) took advantage of the reductive dissolution of hematite and coarse crystallization of magnetite in dilute acetic acid solutions to enhance exchange rates.

For this study, we have selected three reaction pathways to investigate the oxygen isotope fractionation between magnetite and water. These include: (1) reaction of dilute NaCl solutions with fine-grained magnetite, (2) reduction of hematite through reaction with dilute acetic acid (HAc), and (3) oxidation of iron powder in either pure water or dilute NaCl solution. Effective use of acetic acid is restricted to temperatures up to ~400°C because of rapid decomposition to CO$_2$ and CH$_4$ at elevated temperature, whereas magnetite-water and hematite-water interactions become prohibitively slow below ~400°C. Therefore, we are forced to deal with chemical reactions that do not always produce favorable overlaps or continuity in the fractionation data as a function of temperature.

3.2. Experimental

Oxygen isotope exchange experiments in the systems hematite-acetic acid and magnetite-NaCl$_{(aq)}$ were conducted at a variety of temperatures and pressures using the Northrop and Clayton (1966) partial exchange method. Reagent-grade hematite (Alfa Products, Thiokol/Ventron Division, 99.9%, Lot # 042281, ~0.2 to 2 microns in diameter) or magnetite (M: Johnson Matthey, Puratronic iron [II, III], 99.999% Fe$_3$O$_4$; metals basis, Lot # 21173, ~0.25 to 1.5 microns in diameter or m: Lot # S.92743A, ~10 to 30 microns in diameter, mesh-like texture) were reacted with three, and in many cases, four isotopically labeled waters in noble metal capsules. Reagent-grade Fe powder (Fisher, 99.99%, ~1.5 microns) was reacted with two isotopically different solutions each containing 0.1 molal NaCl. For the Fe-H$_2$O system, moderately rapid diffusion of H$_2$ through Pt and even Au capsules above 600°C resulted in magnetite formation, whereas AgPd capsules were needed to facilitate oxide formation at lower temperatures (<500°C).

The acetic acid aqueous solutions were prepared by the addition of the appropriate amount of 100% glacial acetic acid (referred to hereafter as HAc) to each starting water; 0.5 m solutions were made. Similarly, dry NaCl was added to starting waters to give either 0.1 or 0.5 m concentrations. The fluid to solid mass ratios ranged from as low as ~4 to as high as ~50 depending on the temperature-pressure-composition combination. Capsules were weighed to check for leaks before and after being placed overnight in a vacuum oven, and again weighed after each run. Experiments were conducted in standard horizontally mounted cold-seal apparatus using Rene 41 reaction vessels and an aqueous pressure medium. We estimate temperature gradients of <5°C across capsules typically 5 cm long. The time to reach run temperature (controlled to ±1°C) was approximately 15 min or less, and runs were quenched isobarically by passing compressed air stream over the vessel, and also by wrapping the vessel with a wet towel. In all cases, these procedures cooled the vessel to temperatures below 100°C in 5 to 10 min.

At the end of the experiment, each capsule was reweighed to check for leaks. The solid-run products were flushed from each capsule with acetone into a separate glass container, then rinsed several times with deionized water, dried, and stored in a vacuum desiccator. Conversion to magnetite was verified with XRD, SEM, HRTEM, and in a few cases with Mössbauer spectroscopy. SEM observations showed no evidence of crushing of grains in the heat-up cycle unlike that reported for calcite by Tanner et al. (1985), and we observed no fine-grained quench products. In the case of select hematite-acetic acid experiments (e.g., 350°C), large magnetite crystals were harvested for detailed examination by SEM and analysis with the ion microprobe (Fortier et al., 1995). Since each charge consists of thousands of small crystals, the removal of a few large single crystals (~50–150 microns diameter) for ion microprobe analysis does not significantly effect the mass balance of the system, and thus a conventional analysis can be made on the remaining sample.

3.3. Isotopic Analysis

The isotopic compositions of the starting solids and waters are provided in Table 1. Bulk magnetite and hematite powders were analyzed by using a laser-fluorination system at the University of Wisconsin as described by Valley et al. (1995). Samples were pretreated overnight in the sample chamber with ~1000 μmol BrF$_5$ to

remove H_2O and traces of organic compounds. A 32-W CO_2 laser with a defocused laser beam of ~500 μm in diameter was used to heat samples in the presence of ~1000 μmol BrF_5. Typically, 2 to 2.5 mg samples were reacted for 1 to 2 min. An interlaboratory garnet standard, UWG-2, was analyzed before and after the analyses of iron oxides to evaluate oxygen isotope fractionation in the extraction system (Valley et al., 1995). The expected value for this standard is 5.8‰ Vienna Standard Mean Ocean Water (VSMOW). A correction must be applied for all deviations from this value during a particular analytical session. Analyses from only one out of six analytical sessions required a modest correction of +0.16‰. In most cases each run product was analyzed at least twice. Starting waters were equilibrated with CO_2, whose oxygen isotope composition was based on a reference gas calibrated against CO_2 gases equilibrated against both VSMOW and Standard Light Antarctic Precipitation (SLAP); hence there was no need to use an $\alpha_{CO2-H2O}$. These calibrations were done for each analytical session on the ORNL MAT 252 mass spectrometer to monitor accuracy and precision on a day-to-day basis. Analytical errors for starting water $\delta^{18}O$ values were no greater than +0.08‰. Magnetite single crystals from experiments involving reaction of hematite with 0.5m HAc at 350°C were analyzed using a modified Cameca 4f ion microprobe at ORNL using the techniques described in Riciputi and Paterson (1994). The details of this approach and the results have been presented in Fortier et al. (1995). The oxygen isotope ratios in both the iron oxides and water are reported in the standard δ notation versus VSMOW. The precision for oxygen isotope analysis ($\delta^{18}O$) is approximately ±0.05‰ (1σ) for all waters and between ±0.02 to ±0.6‰ for the oxides (magnetite; hematite).

4. EXPERIMENTAL RESULTS

4.1. Mineralogy and Exchange Mechanisms

A detailed mineralogical assessment was made of the run products in this study to gain insight into the possible mechanisms of isotopic exchange (Figs. 1a–1f). The principal characterization methods included SEM, XRD, and optical microscopy, with a select number of samples examined using either HRTEM and/or Mössbauer spectroscopy. Various proportions of binary mixtures of magnetite-hematite and magnetite-Fe were prepared for XRD analysis, providing a basis for the estimation of mineral abundance. Recrystallization, new grain growth, and/or dissolution-precipitation were observed in the run products regardless of the reaction pathway. The extent of conversion of one phase to another, the grain size, and grain habit varied depending on the temperature, starting solution composition (e.g., 0.5 m HAc, 0.1 m NaCl), starting solid and its grain size (magnetite, hematite or Fe powder), and duration of the experiment. Neither TEM nor Mössbauer detected the presence of maghemite or wüstite in the few samples examined (one each representing the three reaction pathways). Additionally, based on XRD, wüstite was not detected in any of the experiments.

In experiments using magnetite as the starting material, Ostwald grain ripening (i.e., grain coarsening at the expense of the dissolution of smaller grains) was prevalent (Figs. 1a and 1b), particularly at the higher temperatures (500°C and above) and in the presence of NaCl (aq). The degree of crystallinity improved with increasing temperature (and duration of the experiment), particularly at 600°C and above where well-formed dodecahedra dominated. It is also important to note that even the well-formed grains exhibited some degree of rounding at crystal edges, and this rounding became more pronounced with decreasing temperature.

The hydrothermal reduction of hematite to magnetite also resulted in considerable magnetite growth depending on temperature, solution composition, and run duration. There did not appear to be any obvious regrowth of the hematite-starting material. At 500 and 600°C a substantial portion of the hematite was converted to magnetite (>80%), but the dodecahedral-shaped grains were of modest size, ranging from less than one micron to only a few microns in diameter. Conversely, reaction between hematite and dilute 0.5 m HAc at lower temperatures (300–400°C) led to profound grain growth with grains attaining diameters as large as 150 microns (Fig. 1d), particularly for the longer duration experiments. Based on these experiments, the optimum condition for magnetite growth appears to be at 350°C in the presence of 0.5 m HAc. At this condition, virtually all of the hematite is transformed to magnetite. This is consistent with the results of Palmer and Drummond (1986) and Bell et al. (1994), who observed enhanced solubility of hematite reacted with dilute HAc in the temperature range of 335 to 350°C.

The oxidation of fine-grain iron metal led to the formation of well-crystallized magnetite (Figs. 1e and 1f). We observed an increase in the extent of crystallinity and grain size with increasing temperature, addition of a mineralizing solution (i.e., NaCl), and run duration. At temperatures of 500°C and above, more than 70% of the Fe that reacted with dilute NaCl was converted to magnetite for run durations in excess of ~240 h. More than 90% of the new magnetite grains exhibited a dodecahedral crystal habit, with the remaining grains taking an octahedral form. At temperatures of 500°C and above, grain sizes ranged from ~0.5 to 5 microns, with a few grains (<5% of the population) attaining diameters of up to 10 microns. At lower temperatures, grain diameters ranged from 0.25 to 2 microns. Virtually all of the grains displayed some form of rounding, which appeared to become more prevalent at the lower temperatures.

There can be no question that isotopic exchange accompanied the recrystallization process associated with each of the reaction pathways. In the Northrop-Clayton partial isotope exchange method, recrystallization of the starting material can be enhanced through the use of electrolyte solutions (e.g., NH_4Cl; NaF). In our study, we employed either NaCl or HAc to promote magnetite recrystallization from either precursor magnetite or Fe metal, or transformation from hematite. However, an ideal isotopic exchange experiment is one controlled exclusively by diffusion (Clayton, 1981; O'Neil, 1986). Diffusion probably contributed significantly to exchange in the high-temperature experiments using magnetite as a starting material, particularly for those grains that were unaffected by grain growth. Based on oxygen diffusion coefficients derived from magnetite-water hydrothermal experiments reported by Giletti and Hess (1988), we estimate that a 1 micron diameter grain would equilibrate (at 100 MPa) in ~100 h at 800°C, 700 h at 700°C and in excess of 5000 h at 600°C. Therefore, at the higher temperatures, coupled mechanisms of regrowth and diffusion contribute to overall exchange. For the run durations used in this study, diffusion-controlled isotope exchange at 600°C and lower involving magnetite would produce only a negligible contribution to the total, far too small to be effective in any partial isotope exchange method. This fact emphasizes the need to promote greater exchange at low temperatures through other means such as recrystallization.

Of real concern is the potential for exchange to occur between hematite and water before its conversion to magnetite. Depending on the extent of exchange and the magnitude of the hematite-water fractionation factor, this contribution could adversely affect the final fractionation factors determined from the partial exchange method. This problem is more acute for the higher temperature experiments. Mineralogical evidence indicates that the hematite did not undergo any obvious recrystallization at any temperature. In fact, at 500°C and above, essentially all of the hematite was converted to magnetite. It is difficult to assess the contribution made by hematite-water exchange via a diffusional mechanism because there are no experimental data comparable to the results reported by Giletti and Hess (1988; 500–800°C) or Castle and Surman (1969; <500°C) for hematite (Cole and Chakraborty, 2001). The total ionic porosities of magnetite and hematite, calculated by the method of Fortier and Giletti (1989), are very similar, i.e., 0.35 versus 0.29, respectively. Thus, we used the magnetite diffusion data as proxies for hematite (assuming a one micron average grain diameter) and estimated the contribution to exchange. For the run conditions used in this study at 500°C (550 h), hematite would undergo only ~4% exchange, less than 1% exchange at 400°C (122 h), and 2% exchange at 350°C (1532 h). According to Zheng (1991), the hematite-water oxygen isotope fractionation factors may be ~1.5‰ lower than those for magnetite-water in the temperature range of 300 to 500°C. Assuming this to be true, the small contributions to exchange estimated from the diffusion mechanism may lower the $10^3 \ln \alpha_{mt-w}$ values by no more than ~0.05‰. We consider this contribution to be negligible given the uncertainty in $10^3 \ln \alpha_{hem-w,}$ and the fact that the magnitude of the contribution is less than the analytical errors estimated for both the starting materials and run products (see Tables 1 and 2).

4.2. Isotopic Fractionation

4.2.1. Partial exchange method

Oxygen isotope fractionation between magnetite, as a starting material, and 0.5 molal NaCl solutions was studied at 300°C, 400°C, 500°C, 600°C, 700°C, and 800°C and pressures of either ~100 or 215 MPa. The results from these partial exchange experiments and associated errors are given in Table 2 with representative examples plotted in Figures 2a and 2b in the conventional Northrop-Clayton form (Northrop and Clayton, 1966). Information required for the mass balance calculations is included in Table 2 as well. Analytical errors ($\pm 1\sigma$) were propagated through the mass balance calculations and assessed by the method of York (1969) as codified by Ludwig (1994) in the calculations of $10^3 (\alpha_i)$ and $10^3 (\alpha_f - \alpha_i)$. The extent of equilibration, determined from the slope (-100/slope of $10^3\alpha_i$ plotted against $10^3(\alpha_f-\alpha_i)$ shown in Figure 2), was 91% for 500°C and $\geq$ 99% for temperatures 600°C and above. At 300°and 400°C, the extent of equilibration was much less, 34.6% and 47.3%, respectively. These more sluggish exchange rates observed at lower temperatures reflect the difficulty encountered in trying to enhance the rate of magnetite recrystallization through reaction with 0.5 molal NaCl, and the fact that oxygen diffusivities are too slow to contribute significantly to overall exchange. Clearly, this was not a problem at the higher

temperatures, where extensive recrystallization and Ostwald ripening were observed.

Magnetite-water oxygen isotope fractionations were also determined from partial isotope exchange experiments where hematite was converted to magnetite after reaction with 0.5 molal HAc (300°C, 350°C, 400°C). It is important to note that this pathway does not adhere strictly to the Northrop-Clayton technique because oxygen is transferred from the solid to the solution. However, because the fluid to solid oxygen mole ratios were on the order of 35 to 40, the net transfer of oxygen is small enough in magnitude that the method can still be used to determine fractionation factors. The results with associated errors are also summarized in Table 2. The percentages of exchange determined from the slopes of the Northrop-Clayton plots are all quite high and vary as a function of temperature and run duration. These percents of exchange are 99.7, 97.8, and 85.1% for 400°C, 350°C, and 300°C, respectively. The extensive amount of oxygen isotope exchange determined in these experiments is consistent with the near-quantitative conversion of hematite to magnetite observed with both SEM and XRD.

The fractionations interpolated from the Northrop-Clayton method range from a maximum of −5.49‰ (at 800°C) to a minimum of −8.88‰ (at 300°C). The standard errors obtained for each fractionation factor are provided in Table 2 and the appropriate error bars have been added to Figure 3a. The temperature trend of these data is clearly evident in Figure 3a, which shows an apparent minimum at around 300 to 400°C. In general, the errors about these fractionations derived from least-squares fits to the Northrop-Clayton plots become larger with decreasing temperature and correlate with a general decrease in the fraction of exchange (increasing slope in plots like those shown in Figure 2). O'Neil (1986) points out that at low fractions of exchange the fractionations determined by the partial isotope exchange method are commonly larger than the "true" equilibrium values. The use of a rapid quench method (cooled to 100°C <5 min), the overall sluggish recrystallization rates of magnetite, and the absence of minor fine-grained quench products suggest that neither the heat up nor the quench processes contributed to the variations observed in the 300 and 400°C fractionations. The link between somewhat less negative fractionations (300 and 400°C magnetite-0.5 m NaCl; Fig. 3a) and lower fractions of exchange may be a consequence of the Northrop-Clayton method.

4.2.2. Fe oxidation pathway

Oxygen isotope fractionation between magnetite, formed from the oxidation of fine iron metal powder, and 0.1 molal NaCl solutions was studied at 500°C, 600°C, 700°C, and 800°C and a pressure of 100 MPa. The results from these exchange experiments are given in Table 3 and plotted in Figure 3b. Each final magnetite δ^{18}O value represents an integrated signal reflecting fractionation resulting from the loss of oxygen from solution during oxidation of iron and magnetite crystal growth. The δ^{18}O value of each final water represents the mean between the initial starting water value and a value calculated from mass balance based on the conversion of iron to magnetite that was calibrated from yields measured during laser fluorination or by XRD. For experiments where the initial fluid-to-
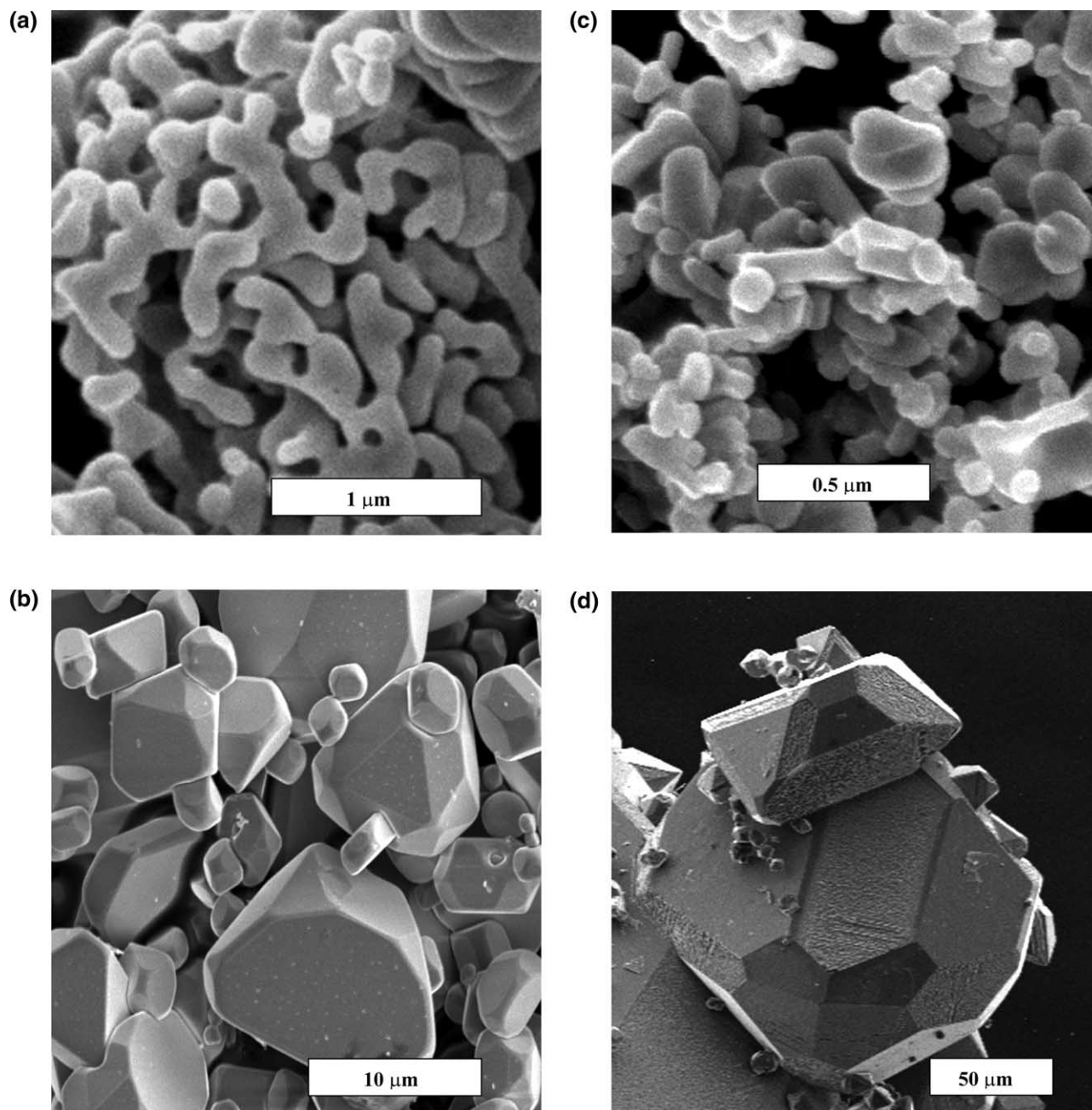
Fig. 1. Scanning electron photomicrographs of starting materials and typical run products: (a) starting magnetite M; (b) magnetite after reaction with 0.5 m NaCl at 800°C for 235 h; (c) starting hematite; (d) magnetite formed after hematite reaction with 0.5 m acetic acid at 350°C for 1532 h; (e) starting iron powder; (f) magnetite formed after reaction of iron powder with 0.1 m NaCl at 700°C for 838 h.

solid oxygen mole ratios were large (29–32 at 500°C, 40–54 at 600°C), the difference between initial and final water $\delta^{18}O$ values is only 0.1 to 0.15‰, whereas for lower fluid-to-solid ratio experiments (700°C, 800°C), this difference varies between ~0.4 and 0.5‰. The errors given for each fractionation factor are based on analytical errors, errors associated with mass balance calculations, and errors resulting from the calculation of mean water values.

The agreement between companion experiments typically ranges from 0.2 to 0.3‰, except for the pair at 500°C which differs by 0.8‰. Regardless of the temperature, the iron metal-solution pair with the lower isotopic starting values (e.g., 0.0 or 2.07‰) always produces the less negative magnetite-solution fractionation. The data exhibit the same general trend of more negative fractionation with decreasing temperature as observed with results from the partial exchange experiments. The extent of the overlap and the deviations between the two data sets are evident in the combined plot of all data given in Figure 3b. At temperatures 600°C and above there is a tendency for the iron oxidation data to either bracket or fall within the error limits of
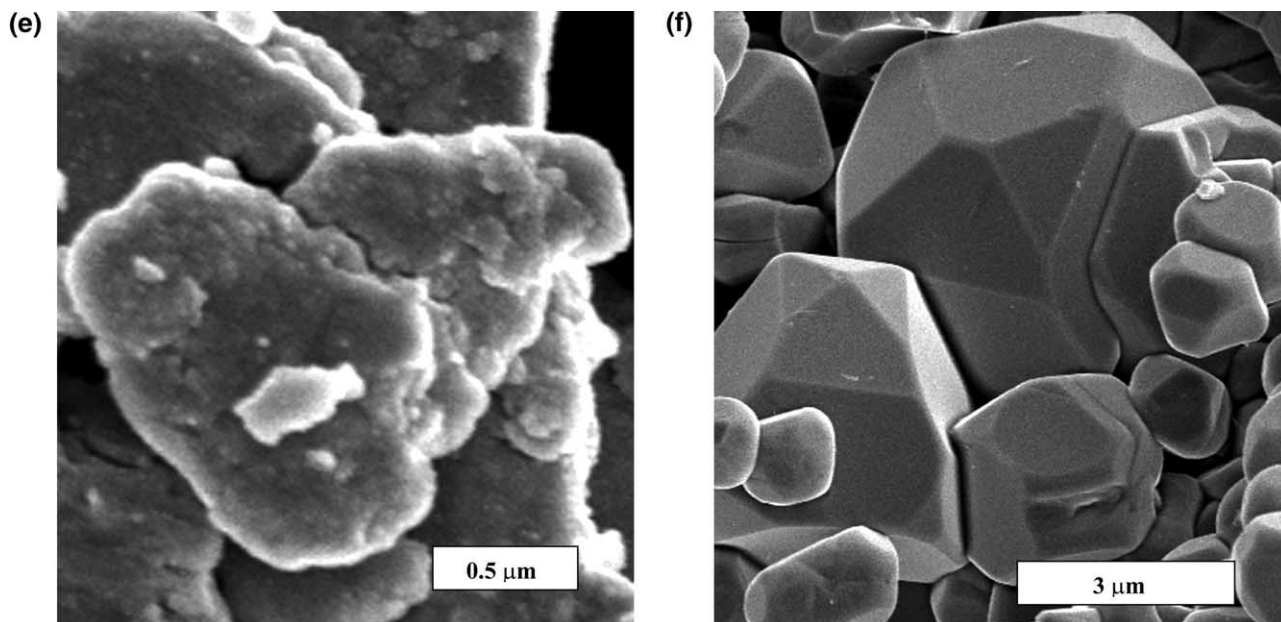
Fig. 1. (Continued)

the partial exchange data. There is a trend at some temperatures (e.g., 500°C, 600°C, 700°C) for the fractionations derived from the oxidation experiments to be somewhat more negative than those from the partial exchange approach.

5. THEORETICAL ASSESSMENT

One of the main objectives in this study was to estimate the oxygen isotope fractionation between magnetite and water, or other phases such as calcite, that can be compared against experimental values. Mössbauer temperature (second-order Doppler) shifts coupled with low-temperature heat capacity measurements can be used to determine the equilibrium isotopic constants (β-factors) for S, O, C, and other elements (e.g., Polyakov, 1997; Polyakov and Mineev, 2000; Polyakov et al., 2001). This technique applies to minerals in which one of the two constituent elements has a Mössbauer-sensitive isotope (e.g., Fe). The first-order thermodynamic perturbation theory relates the β-factor to the difference of masses of the isotopes and the kinetic energy of the atom undergoing isotopic substitution,

$$\ln \beta = \frac{\Delta m_j}{m_j^*} \left(\frac{K_j}{zRT} - \frac{3}{2} \right) \qquad (1)$$

where K is the kinetic energy of the isotope substituted atom, m is the mass of the substituted isotope, * refers to the isotopic-substituted species (^{18}O), $\Delta m = m^* - m$, z is the multiplicity of isotopic substitution, R is the gas constant, T is the absolute temperature, and j subscripts refer to the isotopically substituted element. In the case of magnetite, for the substitution $^{16}O \rightarrow {}^{18}O$, $Fe_3{}^{16}O_4$ and $Fe_3{}^{18}O_4$ are the unsubstituted and isotope substituted forms, respectively, and $z = 4$ (four O atoms in magnetite). Thus Eqn. 1 can be rewritten as

$$\ln \beta = \frac{1}{9} \left(\frac{K_{Ox}}{4RT} - \frac{3}{2} \right) \qquad (2)$$

where K_{Ox} is the vibrational kinetic energy of the oxygen sublattice per mole of the substance.

According to Eqn. 2, determination of the β-factor is reduced to the calculation of the kinetic energy of the oxygen sublattice. Because of the additivity, the total kinetic energy of the crystal lattice of magnetite is equal to the kinetic energy of the iron sublattice plus that of the oxygen sublattice. An immediate consequence of this is

$$K_{Ox} = K - 3K_{Fe} \qquad (3)$$

where K is the total kinetic energy of lattice vibrations; K_{Fe} is the kinetic energy of the iron sublattice.

Calorimetric heat capacity data are used to calculate the total kinetic energy of the crystal lattice, and Mössbauer temperature shifts give the vibrational energy of the sublattice for the element having the Mössbauer-sensitive isotope, in this case iron. A further complicating factor is the need to account for a magnetic field contribution (i.e., magnetite is ferrimagnetic) to the heat capacity versus temperature relationship.

In a harmonic approximation, the kinetic energy can be written as a reciprocal power series in terms of absolute temperature (Thirring expansion),

$$K = RT \left(\frac{3}{2} n + A_1 x - A_2 x^2 + A_3 x^3 + \cdots \right) \qquad (4)$$

where n is the number of atoms in a molecule, equal to 7 for magnetite and $x = 10^6/T^2$. The A_i values for the series can be expressed through statistical moments of the vibrational frequency distribution of a crystal and Bernoulli's number (for

Table 2. Experimental results of oxygen isotope fractionation involving magnetic or hematite starting materials.

Sample No. (a)	Water type (b)	Mass$_{soln}$ (c)	Mass$_{solid}$ (c)	X$_o$H$_2$O (d)	X$_o$Mt (d)	δ^{18}O (‰) Magnetite(e)	δ^{18}O (‰) Water(e)calc	$10^3 (\alpha_i-1)$ (f)	$10^3 (\alpha_f-\alpha_i)$ (g)	$10^3 \ln \alpha_{eq}$ (h)	F (%) (i)
800°C; 100 MPa (235h)											
M-8-1	W-1-0.5	101.75	19.68	0.942	0.058	−11.62 ± 0.24	−6.24 ± 0.03	16.49 ± 0.08	−21.90 ± 0.25	−5.49 ± 0.21	98.9
M-8-2	W-3-0.5	101.87	20.74	0.939	0.061	17.07 ± 0.15	22.99 ± 0.06	−14.33 ± 0.07	8.55 ± 0.18		
M-8-3	W-7-0.5	102.01	20.28	0.940	0.060	2.40 ± 0.02	2.78 ± 0.03	6.77 ± 0.08	−11.94 ± 0.09		
M-8-4	W-8-0.5	101.66	20.20	0.940	0.060	−18.23 ± 0.21	−12.80 ± 0.03	23.72 ± 0.08	−29.32 ± 0.23		
700°C; 105 MPa (838h)											
M-V	W-1-0.5	124.57	25.46	0.938	0.062	−12.39 (±0.11)	−6.12 ± 0.02	16.49 ± 0.08	−22.79 ± 0.14	−6.38 ± 0.16	99.9
M-VI	W-3-0.5	126.40	25.22	0.940	0.060	16.43 ± 0.18	23.04 ± 0.06	−14.33 ± 0.07	7.88 ± 0.21		
M-VII	W-7-0.5	126.15	25.46	0.939	0.061	−3.27 ± 0.33	2.85 ± 0.04	6.77 ± 0.08	−12.88 ± 0.34		
M-VIII	W-8-0.5	125.68	25.41	0.939	0.061	−19.05 ± 0.03	−12.72 ± 0.02	23.72 ± 0.08	−30.14 ± 0.09		
600°C; 107.5 MPa (1798h)											
M-I	W-1-0.5	81.44	21.97	0.920	0.080	−12.31 ± 0.01	−5.67 ± 0.02	16.49 ± 0.08	−23.17 ± 0.08	−6.82 ± 0.44	99.9
M-II	W-3-0.5	81.91	21.97	0.921	0.079	15.61 ± 0.25	22.94 ± 0.06	−14.33 ± 0.07	7.17 ± 0.27		
M-III	W-7-0.5	81.88	21.55	0.922	0.078	−3.65 ± 0.16	3.12 ± 0.16	6.77 ± 0.08	−13.52 ± 0.18		
M-IV	W-8-0.5	81.51	22.00	0.920	0.080	−19.28 ± 0.08	12.09 ± 0.03	23.72 ± 0.08	−30.99 ± 0.12		
500°C; 215 MPa (984h)											
M-9	W-1-0.5	111.33	21.97	0.941	0.059	−12.21 ± −0.21	−6.18 ± 0.02	16.49 ± 0.08	−22.56 ± 0.23	−7.80 ± 0.40	91.0
M-10	W-3-0.5	114.01	21.67	0.943	0.057	14.37 ± 0.02	23.19 ± 0.06	−14.33 ± 0.07	5.71 ± 0.09		
M-11	W-7-0.5	122.06	22.79	0.944	0.056	−3.13 ± 0.03	2.78 ± 0.03	6.77 ± 0.08	−12.67 ± 0.09		
M-12	W-8-0.5	109.33	21.70	0.940	0.060	−17.91 ± 0.03	−12.82 ± 0.02	23.72 ± 0.07	−28.88 ± 0.09		
400°C; 112.5 MPa (1506h)											
M-4-1	W-1-0.5	102.16	24.31	0.929	0.071	−1.67 (±0.03)	−6.71 ± 0.02	16.49 ± 0.08	−11.42 ± 0.09	−7.70 ± 0.83	47.3
M-4-2	W-3-0.5	102.44	24.79	0.928	0.072	11.41 ± 0.16	23.32 ± 0.06	−14.33 ± 0.07	2.69 ± 0.19		
M-4-3	W-7-0.5	103.11	24.95	0.928	0.072	2.75 ± 0.04	2.54 ± 0.03	6.77 ± 0.08	−6.56 ± 0.10		
M-4-4	W-8-0.5	103.01	24.62	0.929	0.071	−5.11 ± 0.12	−13.45 ± 0.03	23.72 ± 0.08	−15.27 ± 0.15		
400°C; 100 MPa (122h)											
H-5	W-1a	453.44	25.64	0.982	0.018	−15.29 ± 0.13	−7.04 ± 0.02	17.40 ± 0.08	−25.70 ± 0.13	−8.54 ± 0.27	99.7
H-7	W-3a	457.05	25.95	0.982	0.018	14.42 ± 0.23	23.42 ± 0.06	−13.46 ± 0.09	4.67 ± 0.24		
H-8	W-4a	448.58	26.80	0.981	0.019	−44.00 ± 0.06	−35.86 ± 0.07	48.51 ± 0.11	−56.95 ± 0.09		
350°C; 100 MPa (1532h)											
m-1	W-1a	500.27	24.17	0.985	0.015	−4.83 ± 0.18	−7.36 ± 0.01	12.64 ± 0.09	−10.09 ± 0.20	−8.47 ± 0.21	48.3
m-2	W-2a	518.81	24.67	0.985	0.015	21.37 ± 0.06	48.02 ± 0.04	−41.25 ± 0.10	5.82 ± 0.13		
m-4	W-4a	502.44	24.28	0.985	0.015	−18.88 ± 0.15	−36.59 ± 0.07	43.61 ± 0.11	−25.23 ± 0.20		
350°C; 100 MPa (1532h)											
H-1	W-1a	503.04	24.39	0.985	0.015	−14.97 ± 0.05	−7.11 ± 0.01	17.40 ± 0.08	25.32 ± 0.05	−8.50 ± 0.07	97.8
H-2	W-2a	495.02	24.60	0.984	0.016	38.19 ± 0.04	47.77 ± 0.04	−36.75 ± 0.09	27.60 ± 0.06		
H-3	W-3a	511.03	26.13	0.984	0.016	14.61 ± 0.05	23.42 ± 0.05	−13.46 ± 0.09	4.85 ± 0.07		
H-4	W-4a	500.38	25.95	0.984	0.016	−41.91 ± 0.67	−36.04 ± 0.11	48.51 ± 0.11	−54.59 ± 0.68		
300°C; 97.5 MPa (1412h)											
M-D-1	W-1-0.5	107.10	25.15	0.930	0.070	1.29 ± 0.08	−6.95 ± 0.02	16.49 ± 0.08	−8.20 ± 0.12	−7.86 ± 0.88	34.6
M-D-2	W-3-0.5	111.86	26.13	0.930	0.070	10.91 ± 0.10	23.37 ± 0.06	−14.33 ± 0.10	2.16 ± 0.15		
M-D-4	W-8-0.5	107.05	25.27	0.929	0.069	−1.32 ± 0.08	13.75 ± 0.03	23.72 ± 0.08	−11.11 ± 0.12		
300°C; 10 MPa (695h)											
H-II	W-2a	450.00	24.58	0.983	0.017	35.63 ± 0.25	47.76 ± 0.05	−36.74 ± 0.09	25.17 ± 0.26	−8.88 ± 0.25	85.1
H-III	W-3a	458.35	24.44	0.983	0.017	13.62 (±0.08)	23.44 ± 0.05	−13.46 ± 0.09	3.85 ± 0.10		
H-IV	W-4a	451.83	23.54	0.984	0.016	−36.57 ± 0.09	−36.13 ± 0.07	48.51 ± 0.11	−48.82 ± 0.12		

(a) δ^{18}O M = 8.85‰, δ^{18}O m = 5.04‰, δ^{18}O H = 9.75‰ (see Table 1 for details).

(b) Starting waters: see Table 1 for isotopic compositions, 0.5 refers for 0.5 molal NaCl, a refers to 0.5 molal acetic acid.

(c) Initial masses (in mg) of solution and solid.

(d) Mole fraction of oxygen in magnetite and H$_2$O that was corrected for dissolved NaCl or HAc. For experiments using hematite as a starting material, mole fractions are adjusted to account for 100% formation of magnetite. This assumption is reasonable for experimental series H-5-8 and H-1-4, but not so for series H-II-IV. Over estimation of oxygen loss to the solution due to magnetite formation, however, leads to an error in the final water oxygen isotope value on the order of only 0.01 to 0.02‰ because of the overwhelming dominance of water oxygen due to the high solution/solid ratios used in the experiments.

(e) Oxygen isotope composition of final magnetite. Errors given as ± 1σ are based on replicate analyses except for values in () that are based on ± 1σ error for garnet standard converted and analyzed along with this particular sample, measured only once.

(f) Calculated isotope composition of final H$_2$O. Errors given as ± 1σ are based on analytical errors for starting materials and final magnetite propagated through the mass balance calculation.

(g) Isotopic difference between initial magnetite (or hematite) and water, minus 1. The ± 1σ errors are based on the analytical errors given in Table 1.

(h) Isotopic difference between final magnetite-H$_2$O difference and the initial magnetite-H$_2$O difference. The ±1σ errors are based on those given in columns 7, 8, and 9.

(i) Equilibrium isotope fractionation factor calculated from Northrop and Clayton (1966) method. The ± 1σ errors are based on both the goodness of fit (scatter about the linear regression) and analytical errors of the isotopic data given in columns 9 and 10 (York, 1969; Ludwig, 1994).

(j) Percent of oxygen isotope exchange, F = 100 × (α$_f$-α$_{eq}$)/(α$_i$-α$_{eq}$).
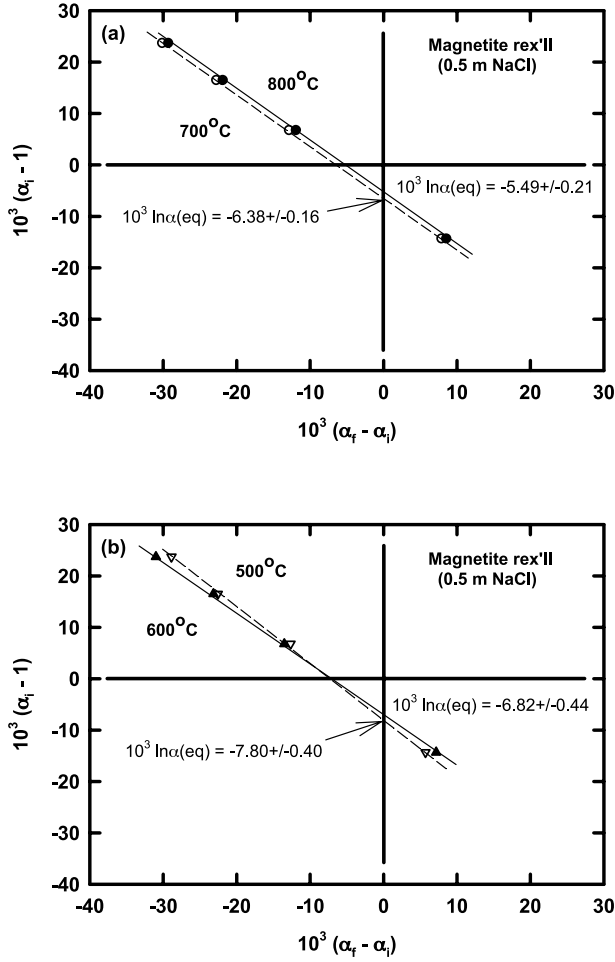
Fig. 2. Representative partial exchange plots after the method detailed by Northrop and Clayton (1966): (a) results from 700 and 800°C magnetite recrystallization experiments using 0.5 m NaCl; (b) magnetite recrystallization pathway for 500 and 600°C using 0.5 m NaCl.

details see Housley and Hess, 1966; Reissland, 1975). The series converges at temperatures that satisfy the inequality

$$kT > (h\nu_m/2\pi), \qquad (5)$$

where h is Planck's constant and ν_m is the maximum frequency in the vibrational spectrum of the crystal. In the harmonic approximation considered here, by the virial theorem, $K = U = 0.5 \, E_{vib}$ (E_{vib} is the vibrational energy of the lattice, U is the potential energy). Combining this with the definition of the heat capacity,

$$C_{Vl} = \left(\frac{\partial E_{vib}}{\partial T}\right)_{Vl}$$

it follows that the contribution of crystal lattice vibrations (C_{Vl}) to the heat capacity is given by

$$C_{Vl} = 2R\left(\frac{3}{2}n - A_1x + 3A_2x^2 - 5A_3x^3 + \cdots\right) \qquad (6)$$

The first terms of the expansions (4) and (6) are classical values

of the vibrational kinetic energy and harmonic heat capacity, equal to $1.5Rn$ and $3Rn$, respectively. The higher members in both expansions are quantum-mechanical corrections to the classical values. The inequality (Eqn. 5) gives the lower bound of convergence for series (4) and (6). For higher temperatures, the limitation on the applicability of expansions (4) and (6) is imposed by anharmonicity. However, it has been shown by Naumov et al. (1997) that expansion (4) for $0.3\theta_D < T < 0.6\theta_D$ (where θ_D is the Debye temperature) can accurately describe the experimental heat capacity data. Eqn. 6 is valid for the lattice component of the heat capacity. However, as noted above, the contribution from magnetization (C_{Vm}) must be considered. Electrical conductivity (C_{Vel}) and anharmonicity (C_{Vanh}) also make minor contributions to the heat capacity. Both increase linearly with temperature. Finally, the total heat capacity of magnetite (C_V) can be given as
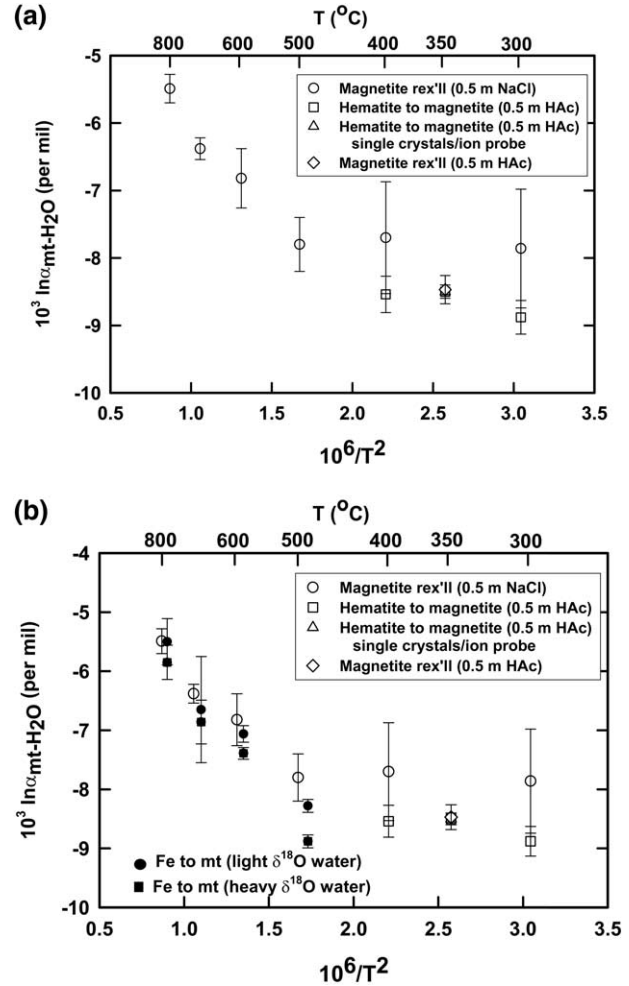

Fig. 3. Plots of 1000 ln α_{mt-H_2O} versus $10^6/T^2$ for: (a) experiments using either magnetite or hematite as staring materials; and (b) combined data sets including the iron to magnetite data. Because of overlap among data points and errors bars, the iron to magnetite data have been offset relative to the data derived from experiments using either magnetite or hematite starting materials.

Table 3. Summary of oxygen isotope fractionation results from experiments involving the oxidation of iron to magnetite.

Run No.	Temp °C	Pressure MPa	Duration Hrs	H$_2$O Type (a)	Mass$_{soln}$ (b)	Mass$_{Fe}$ (b)	X$_o$H$_2$O (c)	X$_o$Mt (d)	δ^{18}O$_{Mt}$ (e)	δ^{18}O$_{H_2O}$ (f)	$10^3 \ln \alpha$ (g)	Wt. % Mt (h)	Method (i)
I-M-D	800	100	235	SMOW	125.38	28.85	0.916	0.084	−5.08 ± 0.21	0.46 ± 0.33	−5.55 ± 0.39	88	Laser
I-M-C	800	100	235	W-7-0.1	125.71	28.58	0.932	0.068	−3.38 ± 0.08	2.47 ± 0.28	−5.85 ± 0.29	75	Laser
I-M-A	700	100	838	W-7-0.1	124.30	25.55	0.921	0.079	−4.05 ± 0.13	2.59 ± 0.37	−6.65 ± 0.39	92	Laser
I-M-B	700	100	838	W-6-0.1	125.00	25.90	0.922	0.078	6.48 ± 0.02	13.41 ± 0.37	−6.86 ± 0.37	90	Laser
I-M-12	600	100	550	W-7-0.1	515.55	26.10	0.985	0.015	−4.87 ± 0.11	2.18 ± 0.08	−7.06 ± 0.14	80	XRD
I-M-13	600	100	550	W-6-0.1	518.22	19.25	0.990	0.010	5.49 ± 0.08	12.95 ± 0.06	−7.39 ± 0.10	75	XRD
I-M-11	500	100	550	W-7-0.1	510.44	32.18	0.983	0.017	−6.05 ± 0.04	2.21 ± 0.10	−8.28 ± 0.11	70	XRD
I-M-10	500	100	550	W-6-0.1	505.37	35.05	0.983	0.017	4.06 ± 0.03	13.02 ± 0.11	−8.88 ± 0.11	65	XRD

(a) Isotopic values for different waters are summarized in Table 1. All solutions have 0.1 m NaCl except SMOW.

(b) Mass, in mg, of starting solution and iron powder.

(c) Mole fraction of oxygen in water after iron conversion to magnetite based on estimated amount of magnetite run product.

(d) Mole fraction of oxygen in magnetite after iron conversion to magnetite based on estimated amount of magnetite run product.

(e) Final oxygen isotope value of magnetite, in per mil. Errors given as ± 1σ are based on replicate analyses.

(f) Final oxygen isotope value of water calculated from mass balance, in per mil. Values represent the mean between the initial water and water calculated from mass balance based on conversion of Fe to magnetite as determined from either yields estimated from laser fluorination or calibration based on XRD. Errors given as ± 1σ about the mean value.

(g) Final oxygen isotope fractionation between magnetite and water, in per mil. Errors given as ± 1σ are based on $\sqrt{(\sigma_{mt}^2 + \sigma_w^2)}$.

(h) Estimated weight percent magnetite in run product.

(i) Method used to estimate weight percent magnetite in run product. Laser refers to the use of oxygen yields from laser fluorination to estimate amount of magnetite in total solid, which also included unreacted iron. XRD refers to the use of X-ray diffraction to estimate the amount of magnetite in the run product based on standard mixtures of iron and magnetite. Estimates based on laser fluorination are good to ±5%, where as the amounts predicted by XRD are good to about 10%.

$$C_V = C_{Vl} + C_{Vm} + C_{Vel} + C_{Vanh} \qquad (7)$$

Based on the work of Holland and Powell (1998), we used the Landau theory for the magnetic term

$$C_{Vm} = \frac{TS_{max}}{2\sqrt{T_c}}(T_c - T)^{1/2} \qquad (8)$$

where $S_{max} = 35$ J/mole K, and Curie temperature $T_c = 848$ K. Because both the electrical conductivity and anharmonic terms are proportional to the first power of temperature, they are combined into one term, $A_{el}T$. Therefore, the variation in heat capacity with temperature follows the relationship

$$C_V = 2R\left(\frac{3}{2}n - A_1x + 3A_2x^2 - 5A_3x^3 + \cdots\right)$$
$$+ A_{el}T + \frac{TS_{max}}{2\sqrt{T_c}}(T_c - T)^{1/2} \qquad (9)$$

where $x = 10^6/T^2$ and $n = 7$. The heat capacity at constant volume was calculated from experimentally measured values of the heat capacity at constant pressure using the Grüneisen relation

$$C_V = C_p(1 - \alpha_T\gamma T) \qquad (10)$$

by assuming that $\alpha_T \sim C_P$ and the Grüneisen parameter (γ) remains constant over the temperature interval of interest (α_T is the thermal expansivity; $\gamma = \alpha_T VB/C_P$, B is the bulk modulus, V is the molar volume). C_V values can be calculated by Eqn. 10 from C_P values. We used the following data at 298.15 K for calculating C_V: $\alpha_T = 2.4 \cdot 10^{-5}$ K^{-1}; $V = 4.452 \cdot 10^{-5}$m^3 ; $B = 178$ GPa; $C_P = 150.79$ J/mole K; $\gamma = 1.26$ (α_T, V and C_p from Kuskov (1993); B derived from Holland and Powell (1990)).

The A_i and A_{el} coefficients obtained from experimental heat capacity values over two different, but slightly overlapping temperature regimes are listed in Table 4. Low-temperature heat capacity experiments were conducted by Westrum and Grønvold (1969) from 5 to 350 K. These data were combined with a second set taken from higher temperature results reported by Grønvold and Sween (1974) for 300 to 1050K. Results presented in Figure 4 indicate that Eqn. 9 and Eqn. 10 provide good agreement with the experimental data for temperatures from 150 to 1050 K (i.e., for the data points used to calculate the coefficients in Eqn. 9), and also allow extrapolations to high temperatures up to 1200 K above the Curie point. A significant difference between experimental and calculated data is observed in vicinity of the Curie point. This difference is not surprising because the assumptions $\alpha_T \sim C_P$ and $\gamma =$ constant are not valid in the vicinity of the phase transition. At temperatures higher than the Curie point, the influence of the phase transition vanishes and the heat capacity values are those of the lattice component only. Good agreement between extrapolated values of the lattice component of the heat capacity and experimental data above the Curie temperature confirms the validity of retrieving the lattice vibration component from the total heat capacity. Based on results of Polyakov (1998), we can neglect the so-called intrinsic anharmonicity in calculating

Table 4. Coefficients A_i and A_{el} for calculating the heat capacity and the total kinetic energy of magnetite based on combined data sets of Westrum and Grønvold (1969) and Grønvold and Sween (1974) (see Eqns. 4 and 9).

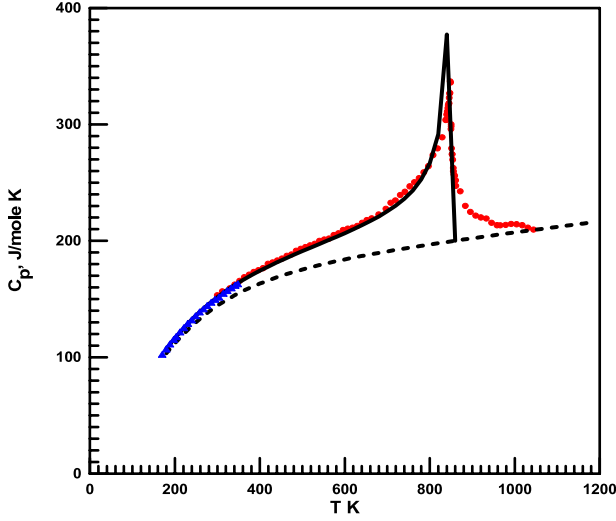| Coefficient	Value	Standard deviation
A_1	0.27300	0.01138
A_2	−1.8407 · 10^{-3}	2.205 · 10^{-4}
A_3	0.9830 · 10^{-5}	2.070 · 10^{-6}
A_{el}	2.7446 · 10^{-2}	3.124 · 10^{-3}

Fig. 4. A comparison of experimental and theoretical data on the heat capacity of magnetite. The calculation is based on data from Westrum and Grønvold (1969; triangles) for 150 to 350 K and data of Grønvold and Sween (1974; circles) for 300 to 1050 K. Solid line is the total lattice and magnetic heat capacity. The dashed line is the lattice heat capacity. The magnetic component was calculated using the Landau theory term (Holland and Powell, 1998). The magnetic component equals zero at temperatures higher than the Curie point according to the Landau theory. The experimental data show the presence of the magnetic contribution to the heat capacity of magnetite in the limited temperature range higher than the Curie point.

the kinetic energy of the lattice vibrations. Consequently, the $A_{el}T$ term drops out and substitution of A_i coefficients from Table 4 into Eqn. 6 provides the Thirring expansion of the lattice vibration kinetic energy of magnetite, given as

$$K = RT(10.5 + (0.2730 \pm 0.01138)x - (1.8407$$
$$\pm 0.2205) \cdot 10^{-3}x^2 + (0.9830 \pm 0.2070) \cdot 10^{-5}x^3) \quad (11)$$

Magnetite is a binary spinel oxide with one Fe^{3+} ion per formula unit on the tetrahedral site (A-site) and one Fe^{3+} and one Fe^{2+} ion on the octahedral sites (B-sites). At temperatures higher than the Verwey transition temperature (≈ 122 K), the B-site iron ion state is not typical for Fe^{3+} nor for Fe^{2+}. This is explained by the high frequency of sixth $3d$ electron jumps between adjacent Fe^{3+} and Fe^2 ions along [110] B-site chains. As a consequence, the properties of both ions are the same and an average valence state is denoted as $Fe^{2.5+}$. Hence, the kinetic energy of the iron sublattice in magnetite can be rewritten as

$$K_{Fe} = K_{Fe}^A + 2K_{Fe}^B \quad (12)$$

where K_{Fe}^A and K_{Fe}^B are the kinetic energies of iron ions in A- and B-sites, respectively.

The kinetic energy of the iron ions can be deduced from the measured temperature (second-order Doppler) shifts in magnetite Mössbauer spectra. The temperature dependence of the shift can be described by the equation (Josephson, 1960; Pound and Rebka, 1960; Lipkin, 1973)

$$\vartheta(T) = \vartheta_o + S \quad (13)$$

where $\vartheta(T)$ is the observed shift, ϑ_o is the temperature-inde-

pendent electronic isomeric shift, and S, the temperature-dependent shift, is related to the kinetic energy through the expression

$$S = -\frac{K_{Fe}}{m_{Fe}c} \quad (14)$$

S is the second-order Doppler shift in Mössbauer spectra measured as the relative speed of the radioactive source, c is the velocity of light, m_{Fe} is the atomic mass of the Mössbauer-sensitive isotope, ^{57}Fe, and K_{Fe} is the kinetic energy of this isotope.

The second-order Doppler shifts for the A- and B-sites in magnetite were measured by De Grave et al. (1993) and Persoons et al. (1993), respectively, and are described by Debye's model with the characteristic Mössbauer temperatures, $\theta_M^A = 640 \pm 25K$ and $\theta_M^B = 570 \pm 15K$. When the characteristic Mössbauer temperature is known, the kinetic energy can be calculated using the Debye-model equation

$$K_{FE} = \frac{9}{16} k\theta_M \left[1 + 8\left(\frac{T}{\theta_M}\right)^4 \int_0^{\theta_M/T} \frac{x^3}{\exp(x) - 1} dx \right] \quad (15)$$

In the framework of the Debye model, the Thirring expansion (4) for K_{Fe} is written as (e.g., see Maradudin et al., 1963)

$$K_{FE} = RT\left(1.5 + \frac{3}{40}\left(\frac{\theta_{Fe}}{T}\right)^2 - \frac{1}{1120}\left(\frac{\theta_{Fe}}{T}\right)^4 \right.$$
$$\left. + \frac{1}{60480}\left(\frac{\theta_{Fe}}{T}\right)^6 - \cdots \right) \quad (16)$$

Substituting the characteristic Mössbauer temperatures for the A- and B-sites in Eqn. 15, one can calculate the kinetic energy of iron atom vibrations in either site and compute the kinetic energy of the iron sublattice, K_{Fe}, by Eqn. 12. The Thirring expansion for K_{Fe} follows from Eqns. 12 and 16. The following polynomial can be derived by conserving the first three terms (as well as in the case of total energy),

$$K_{Fe} = (7.9455 \pm 0.29131) \cdot 10^{-2}x - (3.383$$
$$\pm 0.26242) \cdot 10^{-4}x^2 + (2.2704 \pm 2.8001) \cdot 10^{-6}x^3 \quad (17)$$

where $x = 10^6/T^2$.

If K and K_{Fe} are known, one can find the kinetic energy of the oxygen sublattice and calculate the β-factor of magnetite. The results of this calculation are presented in Table 5. The polynomial expression is given as

$$10^3 \ln \beta = (5.37637 \pm 0.2807)x - (0.04173$$
$$\pm 0.00484)x^2 + (2.01 \pm 0.462)10^{-4}x^3; \, x = 10^6/T^2 \quad (18)$$

Table 5 provides a comparison of β-factors derived from this approach with those calculated from an expression presented by Clayton and Kieffer (1991), obtained through normal statistical thermodynamic calculations for calcite coupled with high temperature calcite-magnetite experiments. A comparison between β's predicted in this study with those of Clayton and Kieffer (1991) indicates that our values are approximately six percent lower in magnitude. Also shown are β-factors for calcite, probably the best constrained of all the minerals and

Table 5. Comparison of oxygen $\beta^{18}O$-factors for magnetite, calcite, quartz and pure water.

Temperature, K	This study Magnetite[a]	Magnetite[b]	Calcite[b]	Quartz[b]	H_2O[c]
1000.00	5.34	5.64	11.38	11.76	11.94
975.00	5.61	5.93	11.95	12.35	12.39
950.00	5.91	6.24	12.56	12.99	12.88
925.00	6.23	6.58	13.22	13.67	13.41
900.00	6.57	6.95	13.93	14.42	13.98
875.00	6.95	7.35	14.71	15.22	14.59
850.00	7.36	7.78	15.54	16.09	15.26
825.00	7.81	8.26	16.45	17.04	15.97
800.00	8.30	8.77	17.44	18.08	16.75
775.00	8.84	9.34	18.52	19.20	17.60
750.00	9.43	9.97	19.71	20.44	18.52
725.00	10.08	10.66	21.00	21.80	19.52
700.00	10.80	11.42	22.428	23.29	20.62
675.00	11.60	12.73	24.00	24.94	21.83
650.00	12.49	13.22	25.74	26.77	23.15
625.00	13.49	14.28	27.67	28.80	24.61
600.00	14.62	15.47	29.82	31.06	26.22
575.00	15.89	16.82	32.23	33.60	27.96
550.00	17.32	18.35	34.93	36.46	29.96
525.00	18.97	20.10	37.97	39.68	32.16
500.00	20.85	22.11	41.42	43.34	34.59
475.00	23.03	24.43	45.34	47.51	37.32
450.00	25.56	27.13	49.84	52.30	40.37
425.00	28.52	30.30	55.03	57.84	43.80
400.00	32.02	34.05	61.08	64.29	47.66

[a] $10^3 \ln \beta^{18}O$ for magnetite from Eq. 18, based on combined heat capacity data of Westrum and Grønvold (1969) and Grønvold and Sween (1974).

[b] $10^3 \ln \beta^{18}O$ data from Clayton and Kieffer (1991).

[c] $10^3 \ln \beta^{18}O$ for liquid water calculated from a fit to data provided by Richet et al. (1977) for temperatures above 650K and β's calculated by combining $10^3 \ln \alpha_{l-v}$ data of Horita and Wesolowski (1994) with β's for isolated water molecule (vapor) from Richet et al. (1977) below 650K. $\beta = 1.537E\text{-}5 \cdot x^3 - 4.926E\text{-}3 \cdot x^2 + 0.00987 \cdot x + 1.00261$ where $x = 10^6/T^2$.

quartz. We have combined our magnetite β values with those for calcite and quartz given by Clayton and Kieffer (1991) and plotted the resulting curves in Figure 5. Experimental values for calcite-magnetite from Chiba et al. (1989) and for quartz-magnetite from Downs et al. (1981) are presented for comparison. Both sets of calculated fractionations exhibit straight lines and project-to-zero fractionation as temperature approaches infinity. Also note that the agreement between the experimental values and these trends is quite good. This is particularly true for the comparison between calculated and experimental calcite-magnetite data.

6. DISCUSSION

6.1. Equilibrium Versus Kinetic Isotope Fractionation

The reactions utilized in this study involved either chemical change, i.e., iron powder oxidized to magnetite and hematite reduced to magnetite, or the recrystallization of magnetite. Therefore, they do not qualify as true isotope exchange reactions. The equilibrium nature of the fractionations can only be inferred, not proven (O'Neil and Taylor, 1969; O'Neil, 1986). In principle, the partial exchange technique should be valid for any percent exchange attained, although with high percentages

of exchange the data are intrinsically more precise (O'Neil, 1986; Chacko et al., 2001). Additionally, if more than one reaction pathway leads to consistent isotopic fractionations derived from partial exchange, then an argument can be made for equilibrium. In this study, the partial exchange method led to percents of exchange, approaching or in excess of 90 in 7 out-of-10 experiments (see Table 2), including both the hematite to magnetite and magnetite recrystallization pathways. At 600°C and above, the percents of exchange exceed 98.9, indicating that magnetite-water in each capsule reached equilibrium according to the definition given by the partial exchange method (Northrop and Clayton, 1966). The agreement between fractionations obtained at 350°C for hematite reduction to magnetite conversion (F>85%) and magnetite recrystallization (F = 48.3%) is identical. The agreement is not close for similar comparisons made at 300 and 400°C, where differences range from 1‰ to ~0.8‰, respectively. Despite the overlap of error bars at 400°C, the significant disagreement between values of $10^3 \ln \alpha$ in this temperature range (300–400°C) somewhat degrades our confidence in knowing the equilibrium fractionation. However, the fractionation at 350°C seems reasonably well constrained (-8.47 ± 0.21 and -8.50 ± 0.07‰) based on the following evidence: (a) identical values obtained from partial exchange data at 350°C from both reaction pathways, and (b) corroborating results from single crystal-water fractionations determined from the ion microprobe analyses of coarse-grained magnetite harvested from hematite-0.5 m acetic acid experiments (-8.6‰; see Fortier et al. (1995)). It is interesting to note that within the error of the ion microprobe measurements (± 0.7‰), the single crystals exhibited no evidence of isotopic zoning, which could arise from kinetic isotope effects due to secular growth.

Kinetic isotope fractionation may have influenced the oxygen isotope partitioning between water and magnetite formed from the oxidation of iron powder. The oxygen isotope fractionations are slightly more negative compared to those determined from the partial exchange method (see Fig. 3b). The unidirectional chemical oxidation of the iron powder to mag-
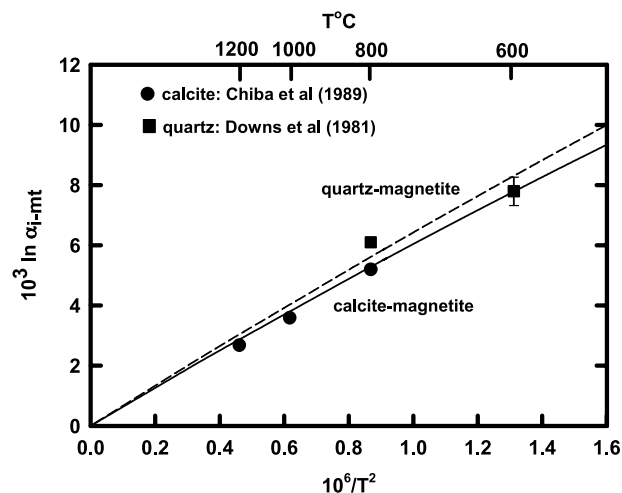

Fig. 5. Comparison of theoretical mineral-(either calcite or quartz) magnetite fractionation factors with experimental values reported by Chiba et al. (1989) for the calcite-magnetite system and Downs et al. (1981) for the quartz-magnetite system.

netite could lead to the preferential enrichment of ^{16}O in the reaction products. The fact that the fractionations are in reasonably good agreement with the partial exchange results suggests that the kinetic isotope contribution is small, and/or magnetite-water partitioning had sufficient time to readjust to fractionations closer to the equilibrium values due to diffusional exchange in the fine-grained reaction products. This latter scenario seems to be consistent with the observations that (a) fractionation factors derived from the two pathways (i.e., iron oxidation and magnetite recrystallization) exhibit closer agreement at temperatures ≥ 600°C where oxygen diffusion rates are relatively rapid, and (b) the differences between fractionations determined from companion iron powder-water experiments (light; heavy water) at a given temperature become noticeably smaller at 600°C and above.

Alternatively, it is possible that fractionation may have been influenced by the formation of another type of iron oxide during the early stages of oxidation, before near-complete conversion to magnetite. The most likely candidate would be wüstite. For the conditions used in our study we might expect the formation of wüstite at temperatures above ~500°C, before the reactants were fully buffered by Ni-NiO. It is also known that wüstite can persist metastably to lower temperatures (L. Anovitz, personal communication). However, we detected no wüstite in the X-ray diffraction patterns obtained from all run products or Mössbauer studies of select run products.

6.2. Temperature Dependence of Equilibrium Fractionation

The present results of magnetite-water fractionation have been fit to a generalized linear least squares regression program employing a number of different temperature terms, $10^3/T$, $10^6/T^2$, $10^9/T^3$, $10^{12}/T^4$ . . . etc. A number of regression scenarios have been examined—regression with and without fixed intercepts, and different combinations of the temperature terms. Because of potential problems associated with the fractionations measured in the iron oxidation experiments, we elected to fit only those data obtained from the two other pathways—magnetite recrystallization plus the hematite to magnetite reaction ($n = 10$; partial exchange). The very best fit to these data was obtained from a regression model containing three temperature terms ($10^6/T^2$, $10^{12}/T^4$, and $10^{18}/T^6$), no intercept, and weighted errors ($1/[\text{total error}]^{1/2}$). The least-squares equation for the combined data sets ($n = 10$) from magnetite recrystallization and hematite to magnetite conversion is given here (see Fig. 6) with the standard errors for each coefficient:

$$1000 \ln \alpha_{mt-w} = -8.984(\pm 0.380)x + 3.302(\pm 0.377)x^2$$
$$- 0.426(\pm 0.092)x^3 \quad R^2 = 0.99 \quad (19)$$

for $300° \leq T \leq 800°C$ where $x = 10^6/T^2$. Clayton et al. (1972) noted that extrapolated fractionation factors in partial exchange experiments involving quartz-water and carbonate-water were larger than equilibrium values determined by complete exchange by 1 to 2‰. Given the potential problem raised by their observations we have also regressed data from the 500 to 800°C experiments that exhibited complete or nearly complete exchange ($n = 4$). This curve is given as
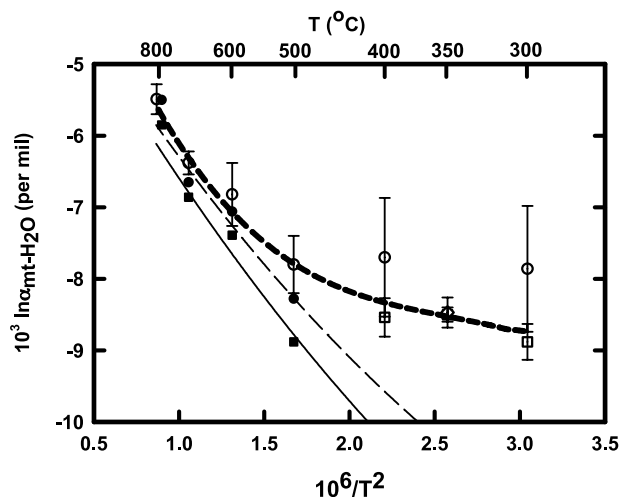

Fig. 6. Plots of $1000 \ln \alpha_{mt-H_2O}$ versus $10^6/T^2$ comparing experimental fractionations with theoretical curves calculated using magnetite β's calculated in this study (thin solid curve) or taken from Clayton and Kieffer (1991; thin dashed curve)) combined with β's for water from Richet et al. (1977). Symbols for our experimental data are the same as given in Figure 3. Bold dashed curve is the best fit to our data considering only the magnetite and hematite starting material experiments, Eqn. 19, and associated errors. See Table 5 for β values of magnetite and "pure" water.

$$1000 \ln \alpha_{mt-w} = -8.284(\pm 0.463)x$$
$$+ 2.181(\pm 0.386)x^2 \quad R^2 = 0.98 \quad (20)$$

for $500 \leq T \leq 800°C$ ($x = 10^6/T^2$). Neither of these two equations predicts a minimum in the temperature range of the experiments. Furthermore, extrapolation of these two equations beyond the experimental temperature ranges used in the curve fits is not advised.

The fractionation curve that describes results obtained from our thermodynamic modeling, i.e., our magnetite β's combined with those for "pure" water (Table 5), is shown in Figure 6 along with our experimental results. Richet et al. (1977) determined β water values by statistical mechanical treatment for isolated water molecules. Below 650 K the β values for water given by Richet et al. (1977) are for water in the form of vapor and have been converted to β's for liquid water using the $10^3 \ln \alpha_{l-v}$ data of Horita and Wesolowski (1994). The β-water values are combined with our estimates of β for magnetite to produce the $10^3 \ln \alpha$ values for magnetite- "pure" water. A fractionation curve derived from the combination of β's given by Clayton and Kieffer (1991) and "pure" water is also presented for comparison. Both of these curves exhibit reasonably close agreement with the experimental results at temperatures 500°C and above but increasingly diverge below this temperature. The Clayton-Kieffer curve plots somewhat closer to the experimental data, but it is important to note that their magnetite β's were estimated by combining the β's for calcite with the calcite-magnetite fractionation factors of Chiba et al. (1989). This approach introduces an experimental bias in these values that we do have with our theoretically derived fractionations. The reasonable agreement observed between the experimental fractionation data and values derived from the combined heat capacity-Mössbauer shift method of Polyakov

(1997) strongly suggests that the thermodynamic approach has great potential for accurately predicting mineral-water fractionations for minerals in which one of the two chemical elements has a Mössbauer sensitive isotope.

6.3. Role of Solutes in Isotopic Fractionation

The differences between theoretically derived mineral-fluid fractionation factors and those determined from experiments serve to illustrate the drawback of such direct comparisons. It is now recognized that dissolved species in the fluid phase can impact fractionation factors to a comparable or larger degree than the largest mineral composition effects (Horita et al., 1995; Hu and Clayton, 2003). This effect applies specifically to fractionations between an aqueous fluid and some other mineral, gas or fluid phase. Because temperature, pressure, and solution composition (i.e., supporting electrolyte and/or dissolved mineral species) all affect the physical properties of water, these three variables act in concert to influence fractionation factors (Horita et al., 2002; Hu and Clayton, 2003). For example, Hu and Clayton (2003) demonstrated that NaCl (aq) systematically changes the oxygen isotope fractionation between quartz and water but has negligible impact on isotopic fractionation between calcite and water. They concluded that the apparent oxygen isotope "salt" effects of NaCl are related to the use of different minerals as reference phases, and that the use of water as an indirect exchange medium will give erroneous fractionations between the two minerals. Thus, mineral-pair fractionation factors derived from different sets of mineral-H_2O experiments may not be internally consistent because the characteristics of the fluid phase may vary with the mineral under investigation and the pressure-temperature conditions. This explains why calcite-quartz fractionations derived from the combination of mineral-water experimental data do not agree well with those determined from direct calcite-quartz experiments.

The differences observed in Figure 6 between the theoretically derived magnetite-water fractionations and our new experimental data may be due, in part, to this "solute" effect. It is certainly reasonable to conclude that iron became complexed as a chloride species during the process of magnetite dissolution and redeposition leading to Ostwald ripening. The combined affects of NaCl (aq) and iron chloride may have been sufficient to produce the kind of "solute" effect described by Hu and Clayton (2003), thereby leading to the differences observed between the "pure" water system and the "magnetite saturated" system. To further illustrate this point, we calculated the β factors for "magnetite" water from our experiments by combining either the β values for magnetite determined in this study or those given by Clayton and Kieffer (1991) with fractionation factors calculated from Eqn. 19. Figure 7 shows the temperature trend of these two sets of β's compared to the values taken from Richet et al. (1977), modified at temperatures below the critical point of water as described above. We have also used fractionation factors for calcite-water and quartz-water from Hu and Clayton (2003) and β values for these two phases (Clayton and Kieffer, 1991) to estimate β "calcite" water and β "quartz" water, respectively. A comparison of these various trends in Figure 6 indicates that all "mineral" water β values plot below the trend given for "pure" water. In
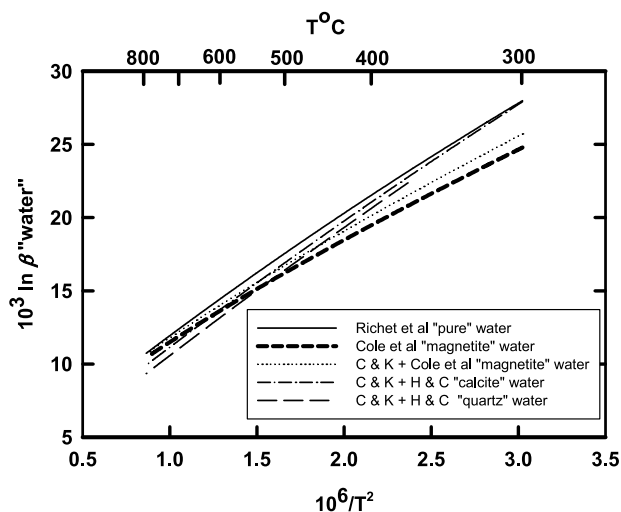

Fig. 7. A comparison of the temperature dependence ($10^6/T^2$) of 1000 ln β "pure" water values taken from Richet et al. (1977) with a number of "mineral-saturated" water β estimates. Cole et al. "magnetite" water refers to the combination of magnetite β values determined in this study with our experimental magnetite-water fractionations factors (heavy dashed curve). C & K + Cole et al. "magnetite-water" refers to the use of β's from Clayton and Kieffer (1991)with our experimental magnetite-water fractionations (light dotted curve). Similar combinations are shown for "calcite" and "quartz" water estimated from combinations of Clayton and Kieffer (1991)β values for these two phases with their respective mineral-water fractionations determined by Hu and Clayton (2003); designated H & C.

the case of magnetite, the β values tend to converge with the pure water curve at high temperature. In the temperature range shown, the "magnetite" water β values deviate from "pure" water by less than 0.5‰ at 800°C to as much as 3‰ at 300°C. This range is similar to the "salt" effect reported by Hu and Clayton (2003). An underestimation of the β_{mt} may also contribute substantially at lower temperature. An opposite trend is observed for both the "quartz" and "calcite" water β values, where the largest difference of approximately 2‰ is observed at 800°C.

6.4. Comparison with Previous Calibrations

As noted in the section describing Previous Work, oxygen isotope fractionation factors currently available in the literature for magnetite-water have been obtained in three principal ways: (1) theoretical calculations using spectroscopic data and the methods of statistical mechanics, (2) laboratory calibration studies, and (3) empirical estimates based on either the increment method or measurements of natural samples where formation conditions are reasonably well-known or highly constrained. Representative curves derived from experiments, theory, and/or empirical methods are shown in Figure 8 along with results from this study.

Agreement among the different fractionation studies varies widely depending on the temperature range of interest. There is moderately good agreement between our results and other experimental results above ~450°C. In particular, the results reported by Bertenrath et al. (1973) and our new results agree to ~0.25‰ or better at temperatures of 500°C and above. The
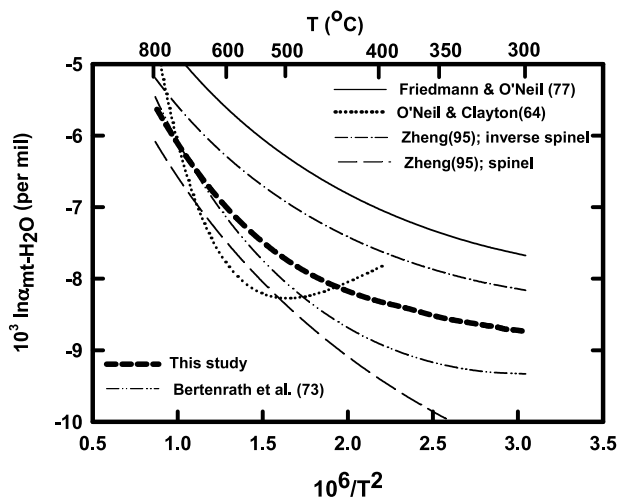
Fig. 8. Plot of $10^3 \ln \alpha_{mt\text{-}H_2O}$ versus $10^6/T^2$ showing the regressed curve to the our new experimental data compared against other fractionations reported in the literature.

deviation becomes progressively larger with decreasing temperature where a difference of ~1‰ is observed at 300°C. The fractionations given by O'Neil and Clayton (1964) have a very steep slope at high temperatures, cross over our results at ~700°C, attain a minimum at approximately 500°C, and cross our curve a second time around 450°C. None of the other curves, including our own in Figure 8, exhibit a minimum in the temperature range of 300 to 800°C.

A comparison between our fractionation factors and those estimated from theoretical or empirical methods serves to illustrate the disparity in agreement among these various results. The curve given by Friedman and O'Neil (1977) has the same overall geometry as our new curve, but predicts 1 to 1.3‰ less negative fractionations. This curve was constructed from the partition ratio of water derived from the experimental calcite-water fractionations and calcite reduced partition function ratios of O'Neil et al. (1969), and the average of Becker's (1971) maximum and minimum values for the reduced partition function ratio for magnetite. The curves estimated from a modified-increment method, detailed by Zheng (1995), tend to bracket our results at temperatures between 300 and 800°C. The upper of these two considers the magnetite structure as inverse-spinel, whereas the lower of the two represents magnetite with a spinel structure. The basic argument Zheng (1995) makes is that magnetite derived from precursor hematite should lead to a fractionation inherited from this phase with a spinel structure. The close similarity in $10^3 \ln \alpha$ values retrieved from our 350°C experiments where both magnetite and hematite were used as starting materials would seem to suggest oxygen is not inherited from the hematite structure. It is true that the fractionations measured from experiments where hematite was converted to magnetite are somewhat more negative than the magnetite recrystallization counterparts (300°C, 400°C). However, we believe this has more to do with the lower fractions of exchange observed in the 300 and 400°C magnetite -0.5 m NaCl experiments.

Although a lower temperature extrapolation (below 300°C) of our results is not highly recommended, it is worth comparing

the position and geometry our curve, with recent results, obtained from low temperature magnetite formation. Zhang et al. (1997) and Mandernack et al. (1999) reported on the oxygen isotope fractionation between water and magnetite formed from thermophilic dissimilatory Fe-reducing bacteria and magneto-tactic bacteria, respectively. These combined data exhibit a linear temperature trend versus $10^6/T^2$, where $1000 \ln \alpha_{mt\text{-}H2O}$ values range from about —1.1‰ at 75°C to +2.5‰ at 5°C. Fractionation results obtained from inorganic magnetite precipitation experiments give values in the range of −4 to 0‰ for temperatures from 90 to 70°C (Horita et al., 1999). An extrapolation of our curve to include these low temperature values would require that it pass through a minimum between approximately 200 and 250°C. The equation given for our experimental data (Eqn. 19), however, will not predict this behavior and should not be used below 300°C.

REFERENCES

Becker R. H. (1971) Carbon and oxygen isotope ratios in iron-formation and associated rocks from the Hammersley Range of Western Australia and their implications. Ph.D. Thesis, University of Chicago.

Bell J. L. S., Palmer D. A., Barnes H. L., and Drummond S. E. (1994) Thermal decomposition of acetate: III. Catalysis by mineral surfaces. *Geochim. Cosmochim. Acta* **58,** 4155–4177.

Bertenrath R., Friedrichsen H., and Hellner E. (1973) Die fraktionierung der sauerstoffisotope $^{16}O/^{18}O$ im systemeisenoxid-wasser. *Fortschr. Mineralogie* **50,** 32–33.

Blattner P., Braithwaite W. R., and Glover R. B. (1983) New evidence on magnetite oxygen isotope geothermometers at 175°C and 112°C in Wairakei steam pipelines (New Zealand). *Isotope Geosci.* **1,** 195–204.

Bottinga Y. and Javoy M. (1973) Comments on oxygen isotope geothermometry. *Earth Planet. Sci. Lett.* **20,** 250–265.

Bottinga Y. and Javoy M. (1975) Oxygen isotope partitioning among the minerals in igneous and metamorphic rock. *Rev. Geophys.* **13,** 401–418.

Castle J. E. and Surman P. L. (1969) The self-diffusion of oxygen in magnetite. The effect of anion vacancy concentration and cation distribution. *J. Phys. Chem.* **73,** 632– 634.

Chacko T. (1993) Experimental studies of equilibrium oxygen and carbon isotope fractionation between phases. In *Experiments at High Pressure and Application to the Earth's Mantle* (ed. R. W. Luth), pp. 357–384. Mineralogical Association of Canada Short Course.

Chacko T., Riciputi L. R., Cole D. R., and Horita J. (1999) A new technique for determining equilibrium hydrogen isotope fractionation using the ion microprobe: Application to the epidote-water system. *Geochim. Cosmochim. Acta* **63,** 1–10.

Chacko T., Cole D. R., and Horita H. (2001) Equilibrium oxygen, hydrogen and carbon isotope fractionation factors applicable to geological systems. In *Stable Isotope Geochemistry* (eds. J. W. Valley and D. R. Cole), Vol. 43, pp. 1–81, Reviews in Mineralogy and Geochemistry.

Chiba H., Chacko T., Clayton R. N., and Goldsmith J. R. (1989) Oxygen isotope fractionations involving diopside, forsterite, magne-

tite, and calcite: Application to geothermometry. *Geochim. Cosmochim. Acta* **53**, 2985–2995.

Clayton R. N. (1981) Isotopic thermometry. In *The Thermodynamics of Minerals and Melts* (eds. R.C. Newton et al.), pp. 85–109, Springer-Verlag.

Clayton R. N. and Kieffer S. W. (1991) Oxygen isotope thermometer calibrations. In *Stable Isotope Geochemistry: A Tribute to Samuel Epstein*, (eds. J. W. Volley et. al.) pp. 3–10 Geochemical Society Special Publication Series.

Clayton R. N., O'Neil J. R., and Mayeda T. K. (1972) Oxygen isotope exchange between quartz and water. *J. Geophys. Res.* **77**, 3057–3067.

Clayton R. N., Goldsmith J. R., and Mayeda T. K. (1989) Oxygen isotope fractionation in quartz, albite, anorthite, and calcite. *Geochim. Cosmochim. Acta* **53**, 725–733.

Cole D. R. and Chakraborty S. (2001) Rates and mechanisms of isotopic exchange. In *Stable Isotope Geochemistry* (eds. J. W. Valley and D. R. Cole), Vol. 43, pp. 83–223, Reviews in Mineralogy and Geochemistry.

Criss R. E. (1999) *Principals of Stable Isotope Distribution*. Oxford University Press.

De Grave E., Persoons R. M., Vandeberghe R. E., and de Bakker P. M. A. (1993) Mössbauer study of the high-temperature phase of Co-substituted magnetites, $Co_xFe_{3-x}O_4$. I. $x \leq 0.04$. *Phys. Rev. B* **47**, 5881–5893.

Downs W. F., Touysinhthiphonexay Y., and Deines P. (1981) A direct determination of the oxygen isotope fractionation between quartz and magnetite at 600 and 800°C and 5 kbar. *Geochim. Cosmochim. Acta* **45**, 2065–2072.

Fortier S. M. and Giletti B. J. (1989) An empirical model for predicting diffusion coefficients in silicate minerals. *Science* **245**, 1481–1484.

Fortier S. M., Cole D. R., Wesolowski D. J., Riciputi L. R., Paterson B. A., Valley J. W., and Horita J. (1995) Determination of equilibrium magnetite-water oxygen isotope fractionation factor at 350°C: a comparison of ion microprobe and laser fluorination techniques. *Geochim. Cosmochim. Acta* **59**, 3871–3875.

Friedman I. and O'Neil J. R. (1977) Compilation of stable isotope fractionation factors of geochemical interest. U. S. Geological Survey. Prof. Paper 440-KK.

Giletti B. J. and Hess K. C. (1988) Oxygen diffusion in magnetite. *Earth Planet. Sci. Lett.* **89**, 115–122.

Grønvold F. and Sween A. (1974) Heat capacity and thermodynamic properties of synthetic magnetite (Fe_3O_4) from 300–1050 K. Ferrimagnetic transition and zero-point entropy. *J. Chem. Thermo.* **6**, 859–872.

Hoffbauer R., Hoernes S., and Fiorentini E. (1994) Oxygen isotope thermometry based on a refined increment method and its application to granulite-grade rocks from Sri Lanka. *Precamb. Res.* **66**, 199–220.

Holland T. J. B. and Powell R. (1990) An enlarged and updated internally consistent thermodynamic dataset with uncertainties and correlations: the system K_2O-Na_2O-CaO-MgO-MnO-FeO-Fe_2O_3-Al_2O_3-TiO_2-SiO_2-C-H_2-O_2. *J. Meta. Geol.* **8**, 89–124.

Holland T. J. B. and Powell R. (1998) An internally-consistent thermodynamic data set for phases of petrological interest. *J. Meta. Geol.* **16**, 309–335.

Horita J. and Wesolowski D. J. (1994) Liquid-vapor fractionation of oxygen and hydrogen isotopes of water from freezing to the critical temperature. *Geochim. Cosmochim. Acta* **58**, 3425–3437.

Horita J., Cole D. R., and Wesolowski D. J. (1995) The activity-composition relationship of oxygen and hydrogen isotopes in aqueous salt solutions. III. Vapor-liquid water equilibration of NaCl solutions to 350°C. *Geochim. Cosmochim. Acta* **59**, 1139–1151.

Horita J., Cole D. R., Valley J. W., and Hayashi K.-I. (1999) Oxygen isotope fractionation of iron oxide minerals at low temperatures. *Geol. Soc. Am. Ann. Mtg., Abstracts with Prog.* **31**, A-276.

Horita J., Cole D. R., Polyakov V. B., and Driesner T. (2002) Experimental and theoretical study of pressure effects on hydrogen isotope fractionation in the system brucite-water at elevated temperatures. *Geochim. Cosmochim. Acta* **66**, 3769-3788.

Housley R. M. and Hess F. (1966) Analyses of Debye-Waller-factor and Mössbauer thermal shift measurements I. General theory. *Phys. Rev.* **146**, 517–526.

Hu G. and Clayton R. N. (2003) Oxygen isotope salt effects at high pressure and high temperature, and the calibration of oxygen isotope geothermometers. *Geochim. Cosmochim. Acta* **67**, 3227–3246.

Javoy M. (1977) Stable isotope geothermometry. *J. Geol. Soc. London* **133**, 609–636.

Josephson B. D. (1960) Temperature-dependent shift of γ-rays emitted by a solid. *Phys. Rev. Lett.* **4**, 341–342.

Kieffer S. W. (1982) Thermodynamic and lattice vibrations of minerals: 5. Applications to phase equilibria, isotopic fractionation, and high-pressure thermodynamic properties. *Rev. Geophys, Space Phys.* **20**, 827–849.

Kuskov O. L. (1993) THERMOSEIM database: thermal, electrical and caloric properties of minerals at 1 bar and 298.15K. Theoretical Geochemistry Program, Institute of the Earth Sciences, Uppsala University, 41 p.

Lipkin H. J. (1973) *Quantum Mechanics: New Approaches to Selected Topics* North-Holland, Pub. Co., Amsterdam.

Ludwig K. R. (1994) ISOPLOT: A plotting and regression program for radiogenic-isotope data, Version 2. **71**, U. S. Geological Survey Open-File Report 91–445.

Mandernack K. W., Bazylinski D. A., Shanks W. C., III, and Bullen T. D. (1999) Oxygen and iron isotope studies of magnetite produced by magnetotactic bacteria. *Science* **285**, 1892–1896.

Maradudin A. A., Montrol E. W., and Weiss G. H. (1963) *Lattice Dynamics in the Harmonic Approximation*. Academic Press.

Matthews A. (1976) Magnetite formation by the reduction of hematite with iron under hydrothermal conditions. *Am. Min.* **61**, 927–932.

Naumov V. N., Frolova G. I., and Atake T. (1997) The extraction of phonon and electron properties from experimental heat capacity with new approximation based on high temperature expansion. *Thermochim. Acta* **299**, 101–108.

Northrop D. A. and Clayton R. N. (1966) Oxygen isotope fractionations in systems containing dolomite. *J. Geol.* **74**, 174–196.

O'Neil J. R. (1963) Oxygen isotope fractionation studies in mineral systems. Ph.D. Thesis, University of Chicago.

O'Neil J. R. (1986) Theoretical and experimental aspects of isotopic fractionation. In *Stable Isotopes in High Temperature Geological Processes* (eds. J. W. Valley et al.), Vol. 16, pp. 1–40, Reviews in Mineralogy.

O'Neil J. R and Clayton R. N. (1964) Oxygen isotope geothermometry. In *Isotopic and Cosmic Chemistry* (eds. H. Craig et al.), North-Holland, Pub. Co., Amsterdam.

O'Neil J. R. and Taylor H. P. (1969) Oxygen isotope equilibrium between muscovite and water. *Am. Mineral.* **52**, 1414–1437.

O'Neil J. R., Clayton R. N., and Mayeda T. K. (1969) Oxygen isotope fractionation in divalent metal carbonates. *J. Chem. Phys.* **51**, 5547–5558.

Palmer D. A. and Drummond S. E. (1986) Thermal decarboxylation of acetate. Part I. The kinetics and mechanism of reaction in aqueous solution. *Geochim. Cosmochim. Acta* **50**, 813–823.

Persoons R. M., De Grave E., de Bakker P. M. A., and Vandenberghe R. E. (1993) Mössbauer study of the high-temperature phase of Co-substituted magnetites, $Co_xFe_{3-x}O_4$.II. $x \geq 0.1$. *Phys. Rev. B* **47**, 5894–5905.

Polyakov V. B. (1997) Equilibrium fractionation of the iron isotopes: Estimation from Mössbauer spectroscopy data. *Geochim. Cosmochim. Acta* **61**, 4213–4217.

Polyakov V. B. (1998) On anharmonic and pressure corrections to the equilibrium isotopic constants for minerals. *Geochim. Cosmochim. Acta* **62**, 3077–3085.

Polyakov V. B. and Mineev S. D. (2000) Mössbauer spectroscopy as applied to isotopic geochemistry: II The β^{34}S-factor in pyrite and β-^{18}O factor in hematite. *Geochem. Int.* **38**, 831–837.

Polyakov V. B., Mineev S. D., Gurevich V. M., Khramov D. A., Gavrichev K. S., Gorbunov V. E., and Golushina L. N. (2001) The use of Mössbauer spectroscopy and calorimetry for determining isotopic equilibrium constants, hematite. *Russ. J. Phys. Chem.* **75**, 912–916.

Pound R. V. and Rebka G. A., Jr. (1960) Variation with temperature of the energy of recoil-free gamma rays from solids. *Phys. Rev. Lett.* **4**, 274–275.

Reissland J. (1975) *The Physics of Phonons*. Benjamin/Cummings.

Richet P., Bottinga Y., and Javoy M. (1977) A review of the hydrogen, carbon, nitrogen, oxygen, sulphur, and chlorine stable isotope fractionation among gaseous molecules. *Ann. Rev. Earth Planet. Sci.* **5,** 65–110.

Richter R. and Hoernes S. (1988) The application of the increment method in comparison with experimentally derived and calculated O-isotope fractionations. *Chem. Erde.* **48,** 1–18.

Riciputi L. R. and Paterson B. A. (1994) High spatial resolution measurement of O isotope ratios in silicates and carbonates by ion microprobe. *Am. Min.* **79,** 1227–1230.

Rowe M. W., Clayton R. N., and Mayeda T. K. (1994) Oxygen isotopes in separated components of CI and CM meteorites. *Geochim. Cosmochim. Acta* **58,** 5341–5347.

Schütze H. (1980) Der Isotopenindex—eine Inkrementenmethode zur näherungsweisen Berechnung von Isotopenaustauschgleichgewichten zwischen kristallinen Substanzen. *Chem. Erde.* **39,** 321–334.

Tanner S. B., Kerrick D. M., and Lasaga A. C. (1985) Experimental kinetic study of the reaction: calcite + quartz = wollastonite + CO$_2$, from 1 to 3 kilobars and 500° to 850°C. *Am. J. Sci.* **285,** 577–620.

Taylor H. P., Jr. (1997) Oxygen and hydrogen isotope relationships in hydrothermal mineral deposits. In *Geochemistry of Hydrothermal Ore Deposits* (ed. H. L. Barnes), pp. 229–302, John Wiley & Sons.

Valley J. W. and Cole D. R. eds. (2001) *Stable Isotope Geochemistry*, Volume 43. Reviews in Mineralogy and Geochemistry.

Valley J. W., Kitchen N., Kohn M. J., Nierdorf C. R., and Spicuzza M. J. (1995) UWG-2, a garnet standard for oxygen isotope ratios: Strategies for high precision and accuracy with laser heating. *Geochim. Cosmochim. Acta* **59,** 5223–5231.

Valley J. W., Graham C. M., Harte B., Eiler J. M., and Kinney P. D. (1998) Ion microprobe analysis of O, C and H isotope ratios. In: (ed. M. McKibben et al.) Soc. Econ. Geologists Rev. Econ. Geol. **7,** 73–98.

Westrum R. F., Jr. and Grønvold F. (1969) Magnetite (Fe$_3$O$_4$) heat capcity and thermodynamic properties from 5 to 350K, low temperature transition. *J. Chem. Thermo.* **1,** 543–557.

York D. (1969) Least-squares fitting of a straight line with correlated errors. *Earth Planet. Sci. Lett.* **23,** 387–396.

Zhang C., Liu S., Phelps T. J., Cole D. R., Horita J., Fortier S. M., Elless M., and Valley J. W. (1997) Physicochemical, mineralogical, and isotopic characterization of magnetite-rich iron oxides formed by thermophilic bacteria. *Geochim. Cosmochim. Acta* **61,** 4621–4632.

Zheng Y. F. (1991) Calculation of oxygen isotope fractionation in metal oxides. *Geochim. Cosmochim. Acta* **55,** 2299–2307.

Zheng Y. F. (1995) Oxygen isotope fractionation in magnetites: structural effect and oxygen inheritance. *Chem. Geol.* **121,** 309–316.